

THERMO BAT

A Ferrosilicon Latent Heat Thermophotovoltaic Battery

Project ID: 101057954

Call: HORIZON-EIC-2021-TRANSITION-CHALLENGES-01

DG / Agency: EISMEA

01/06/2022 - 31/05/2026

D3.3

Report on characterization of TPV cells and modules

Due date of deliverable: 30 May 2024

Actual submission date: 24 December 2024

Partner responsible of this deliverable: UPM

Dissemination Level		
PU	Public	X
CO	Confidential, only for members of the consortium (incl. the Commission Services)	

Intentionally blank page

Abstract

This report focuses on the characterization of the thermophotovoltaic (TPV) cells and modules developed in Work Package 3 (WP3) of the Thermobat project. It also covers the progress made in the development of the point-contact TPV cell, which has been carried out at the Solar Energy Institute using a laser-firing technique. Specifically, this report compares an initial TPV cell prototype, fabricated using a standard technique, with a more advanced cell structure that incorporates several enhancements designed to significantly improve efficiency. Furthermore, these cells are here compared to the commercial Germanium (Ge) TPV devices currently used in the development of the high-temperature thermal battery within the project. This report details the advanced cell structure, provide insights into the fabrication process, and present experimental characterization results, which together constitute the core of the work presented here.

Within the number of iterations of cell structures designed, manufactured and characterized in the framework of WP3, the latest version is based on an upright semiconductor structure that includes a stack of three layers (a-SiC_x:H / Al₂O₃ / a-SiC) on the rear side with the triple purpose of: 1) surface passivation that enables a significant reduction of the surface recombination velocity, 2) provision of the source of doping at the rear metal-semiconductor contact activated by laser ablation aimed at the reduction of this series resistance component, and 3) improvement of the rear TPV cell mirror for the reflection of unabsorbed light that enters the front cell and is transmitted through the whole cell thickness. The numerous TPV cell fabrication and characterization experiments, firstly, carried out on a simplified conventional test structure on highly doped ($2 \cdot 10^{17} \text{ cm}^{-3}$) Ge substrate, and, eventually, on a more advanced architecture known as passivated emitter rear contact (PERC). Three different doping concentration substrates have been used to implement these PERC devices: a highly doped substrate with $2 \cdot 10^{17} \text{ cm}^{-3}$, a medium doped substrate with $2 \cdot 10^{16} \text{ cm}^{-3}$, and a lowly doped substrate of $2 \cdot 10^{15} \text{ cm}^{-3}$. The PERC structures include laser-fired rear point contacts, which have allowed reaching an efficiency of 11.2% and a power density of 1.43 W/cm^2 at $1,544 \text{ }^\circ\text{C}$ for the medium doping substrate. These results have been possible thanks to the improvements already anticipated in the deliverable D3.1, regarding the use of less doped substrates, dielectric layers and punctual laser ablated contacts in the rear, meant to improve reflectivity in the out-of-band spectral range and surface passivation, while producing a reasonably good contact resistance. The optical and electrical characterization of the most representative TPV cell batches that have been fabricated is shown and discussed in this report. Such experimental results have allowed us to thoroughly understand the loss mechanisms corresponding to surface passivation, device recombination, series resistance, lack of reflectivity of the rear side of the cell, free carrier absorption, etc. This exhaustive experimental work, together with the modeling efforts devoted to deepening the understanding of the characterization results, has followed an iterative cell fabrication-and-characterization strategy. All these cell iterations have systematically incorporated TPV cell technological improvements as they were being gradually understood, providing the necessary feedback for the design of more performant homemade TPV cells. Our Ge cells have so far increased the efficiency of commercial cells by more than three times. The analysis of the electrical and thermal behavior of the TPV devices has been

instrumental not only in deepening the understanding of TPV system performance but also in shaping strategic planning and identifying potential technological advancements. These insights provide a roadmap for future experiments aimed at achieving—and potentially exceeding—the milestones set for this project.

This report also presents the experimental characterization of the TPV module, and the efforts made to achieve key milestones during its development. The TPV module is composed of interconnected minimodules, which serve as the fundamental cell-interconnection units. Each minimodule consists of 10 cells arranged in a series-parallel configuration: in our case, two sets of five parallel-connected cells are connected in series. To mitigate power losses in the full TPV module—comprising numerous interconnected minimodules—under inhomogeneous illumination, each minimodule includes a bypass diode. This bypass diode, designed and fabricated in-house from a Ge p-n junction, exhibits a relatively low leakage current of 24 mA/cm² under reverse bias during normal TPV module operation. Under high forward bias conditions (expected when the diode activates to bypass a poorly illuminated or defective minimodule) shows a low voltage forward drop of approximately 0.6 V at more 10 A (which precise value depends on the emitter temperature).

The report also analyzes the electrical performance of the minimodules under high irradiance conditions, evaluated using a flashlight solar simulator. The resulting current-voltage curves, which include the interconnection of multiple minimodules, provide insights into potential issues such as current mismatch and series resistance. A thermal study of the minimodules has been conducted to evaluate their electrical performance as a function of operating temperature. This analysis provides valuable insights into their expected performance in a real TPV system, where the cell operating temperature may increase if the capacity to dissipate heat from the incandescent emitter is limited.

A total of 18 minimodules, comprising a total of 180 Ge TPV cells, have been successfully fabricated and tested in our laboratory. During testing, we measured a total power output of 74 W under 100 suns, equivalent to the irradiation of approximately 1200 °C graphite emitter with a view factor of 1. The high yield achieved in the fabrication process demonstrates that achieving high power levels is straightforward. However, the manufacturing of larger quantities has been intentionally postponed mitigating the risk of encountering unforeseen challenges during real-condition characterization in WP4, which might require re-design. By adopting this approach, we retain a significant stock of cells that can be used for assembling alternative module configurations if necessary. If no issues are identified, we can confidently scale up production to manufacture a larger number of cells, enabling the generation of even higher power levels.

Intentionally blank page

Table of Contents

Abstract	3
Introduction.....	7
Cell characterization	9
Cell description.....	9
Electrical characterization of I-V curves under dark conditions	11
Electrical characterization of I-V curves under high-irradiance flashlight.....	13
Quantum efficiency characterization	16
Optical characterization.....	18
High temperature TPV cell efficiency characterization	20
Simulations and next steps	24
Module characterization	28
Dark I-V characterization.....	28
High irradiance I-V characterization	31
Thermal characterization.....	35
Conclusions	38
References	39

Introduction

Thermophotovoltaic (TPV) converters are devices that produce electricity directly from radiant heat [1], [2]. In THERMOBAT, TPV devices will be used to harness the thermal energy that is stored at very high temperatures in a latent heat thermophotovoltaic (LHTPV) battery demonstrator [3]. The final goal is to develop a 1 kW TPV generator that can be integrated in the complete LHTPV system to demonstrate its feasibility.

TPV converters are similar to solar cells in that they directly convert infrared photons into electricity through a photovoltaic (PV) cell. However, unlike conventional solar PV systems, TPV devices can achieve higher conversion efficiencies by reflecting low-energy photons (those unable to generate electricity in the cell) back to the heat source. Although TPV converters have been under development since the late 1960s, it was not until the mid-1990s that high-quality infrared semiconductors, such as InGaAs and GaSb, became available. These advancements enabled the demonstration of high conversion efficiencies exceeding 20% [4].

This project proposes the development of the first prototype of a complete medium-scale LHTPV battery system. To achieve this, it aims to recover thermal energy stored as heat using a 1 kW TPV system, which requires a significant number of TPV cells—undoubtedly the most expensive component per unit volume in the entire system. Since initial real-scale prototype designs need to have some flexibility, allowing variations in the arrangement and/or interconnection of the cells, the use of low-cost devices, such as those based on Ge, was proposed. This indirect bandgap material is based on cheaper and more abundant substrates than those of InP, which are required for the manufacture of InGaAs TPV cells. Although the efficiency and power density using Ge cells is clearly lower than InGaAs, their low cost makes them an ideal option at this stage of development. Beyond these techno-economic considerations, this project aims to push the technology to limits never before explored with Ge cells for their use in TPV applications. Hence, this type of cells arises as a strong candidate for use in high-temperature storage systems based on LHTPV batteries with truly competitive efficiencies and, more importantly, power densities comparable to those produced by current InGaAs technology.

This report presents a comparative assessment of the electrical and optical characterization of five distinct TPV cells, four of which were fabricated in-house, alongside a commercially manufactured cell. The first cell serves as a basic benchmark device for performance comparison (with a $2 \cdot 10^{17} \text{ cm}^{-3}$ substrate and a simplified structure). The second cell ($2 \cdot 10^{17} \text{ cm}^{-3}$ and PERC structure) incorporates various advanced features, including rear passivation layers and laser-fired point contacts, representing a significant step forward for TPV application. The third cell ($2 \cdot 10^{16} \text{ cm}^{-3}$ and PERC structure) builds upon the second, utilizing a medium doped germanium (Ge) substrate intended to reduce the absorption of the low energy photons by the free carrier absorption mechanism; this way, enhancing the reflected component of the unabsorbed light back to the TPV emitter. The fourth cell ($2 \cdot 10^{15} \text{ cm}^{-3}$ and PERC structure) explores an even lower substrate doping with the same intention as the third one. Finally, the fifth device is a commercial cell (high doping concentration and simplified structure) to be

Page 7 of 39

integrated into the minimodules meant to constitute the TPV generator in our high-temperature thermal battery.

The characterization techniques employed to compare the different TPV cell technologies are among the most widely used and valuable methods for evaluating photovoltaic devices. These techniques provide critical insights into the electrical and optical performance of the cells, enabling a thorough comparison of their respective strengths and weaknesses:

- *I-V* curves under illumination obtained with a pulsed flashlight from the concentrated-light simulator setup that emulates the high irradiance generated by the incandescent material stored in the crucible of the energy-storing unit.
- Measurement of the quantum efficiency, which is a technique that combines both optical and electrical characterization that allows determining the ratio between the photogenerated electrons collected through the cell terminals and the photons of different wavelengths impinging on the cell surface.
- Optical characterization, performed in this case using a Fourier Transform Infrared Spectroscopy (FTIR) technique, intended for knowing the reflection spectrum obtained at the surface of the cell, which can be resolved up to very long wavelengths (>20 μm). This reflectivity is a function of several cell features, such as anti-reflecting coatings (ARC), metal grid surface, absorption in the semiconductor or reflection at the rear side mirror.
- Finally, *I-V* curves also measured under high irradiance conditions, but using the TPV efficiency setup developed at the Solar Energy Institute (IES) at UPM [5], where the *I-V* curve is measured under the effect of the high temperature emitter located in a vacuum chamber.

The characterization of TPV cells, their interconnections within minimodules, and the complete TPV modules formed by multiple interconnected minimodules is essential to understand loss mechanisms and gain a deeper understanding of each component. This knowledge is crucial for optimizing the system in subsequent prototyping stages. The performance analysis of individual cells and interconnection configurations, allows pinpointing inefficiencies and identifying areas for improvement, leading to optimized designs and manufacturing processes that produce more efficient, reliable, and cost-effective TPV systems.

This report includes detailed measurements of all TPV system components, starting with individual cells, bypass diodes, minimodules, and their electrical interconnections, providing insights into the expected performance of the complete TPV system. The experimental characterization results here shown include dark and concentrated illumination *I-V* curves. The latter are obtained from the pulsed light of a flash simulator and from the incandescent emitter of a high-temperature TPV efficiency characterization setup. Additionally, the electrical behavior of modules following

thermal cycling is assessed to simulate the thermal expansions that occur under real operational conditions.

In summary, in parallel with efforts to develop and characterize the complete TPV system, work has focused on enhancing rear point-contact cells based on Ge using more cost-effective manufacturing processes with a high-speed laser-firing system that allows rear surface passivation for reducing recombination and enhance open-circuit voltage (V_{oc}) and good rear mirror quality for the unabsorbed infrared light, all together with a good contact resistance. Significant progress has been achieved in the second year of the project, with efficiency improvements from 2.3% to 11.2% and an increase in power density from 0.48 W/cm² to 1.43 W/cm² at an operating temperature of 1,544 °C.

Cell characterization

This section provides a comprehensive analysis of the performance and characteristics of the studied TPV cells. It begins with a brief description of the four types of TPV cells investigated, setting the stage for a deeper exploration of their properties. Following this, the electrical characterization of the current-voltage (I - V) curves is presented under dark conditions, offering insights into the devices' baseline performance. Subsequently, the I - V characterization under high-irradiance flashlight conditions is discussed, highlighting their electrical behavior under equivalent TPV illumination. The analysis then moves to the quantum efficiency characterization, providing a detailed assessment of the devices' spectral response. This is complemented by an optical characterization focusing on infrared reflectivity, measured using FTIR spectroscopy, which explores the cells' interaction with thermal radiation. Finally, the section concludes with the high-temperature I - V curve characterization and efficiency evaluation, emphasizing the devices' performance when subject to elevated emitter temperatures.

Cell description

With respect to the TPV cells to be used in the final system of the Thermobat project, 550 1 cm² units have been acquired. Their structure is shown in Figure 1(a), where most of the epitaxial and fabrication data are not displayed because the supplier does not disclose neither the semiconductor structure, nor the device fabrication details. This cell, referred to as "commercial" from now on, is based on a p-type Ge substrate with thick silver metallic contacts and a 200 nm gold termination to prevent oxidation and facilitate bonding. Additionally, the cell features layers that allow for the passivation of the front layer, as well as an ARC optimized for the near infrared spectrum from TPV operation.

Following this, two other cell structures manufactured at IES-UPM during these two first two years of the project are also shown for comparison. The first one, whose structure is represented in Figure 1(b), is denoted as "conventional" and consists of a simple structure

featuring a fully gold-coated back contact and no rear passivation layers. The fabrication process of this conventional cell is carried out only employing photolithography, instead of the more sophisticated laser-firing technique used in the advanced TPV cells described below. These samples are used as a cell technology starting point in this report, serving as reference for the development of technological improvements aimed to increase TPV efficiency and power density. This third structure, shown in Figure 1(c), representing the current progress through more performing Ge TPV cells, is similar to the classical solar cell design known as passivated emitter rear contact (PERC). Following this design, three different doping concentration substrates with 10^{17} , 10^{16} cm^{-3} and 10^{15} have been used to study the impact on cell performance. In this study, they are referred to as “PERC_17” , “PERC_16” and “PERC_15, respectively. The TPV cells conceived with this PERC design include the rear passivation layers with which rear point contacts are developed by laser ablation, as illustrated in Figure 1(c). This cell architecture allows enhancing reflectivity in the infrared region while maintaining good surface passivation through the formation of a back surface field (BSF).

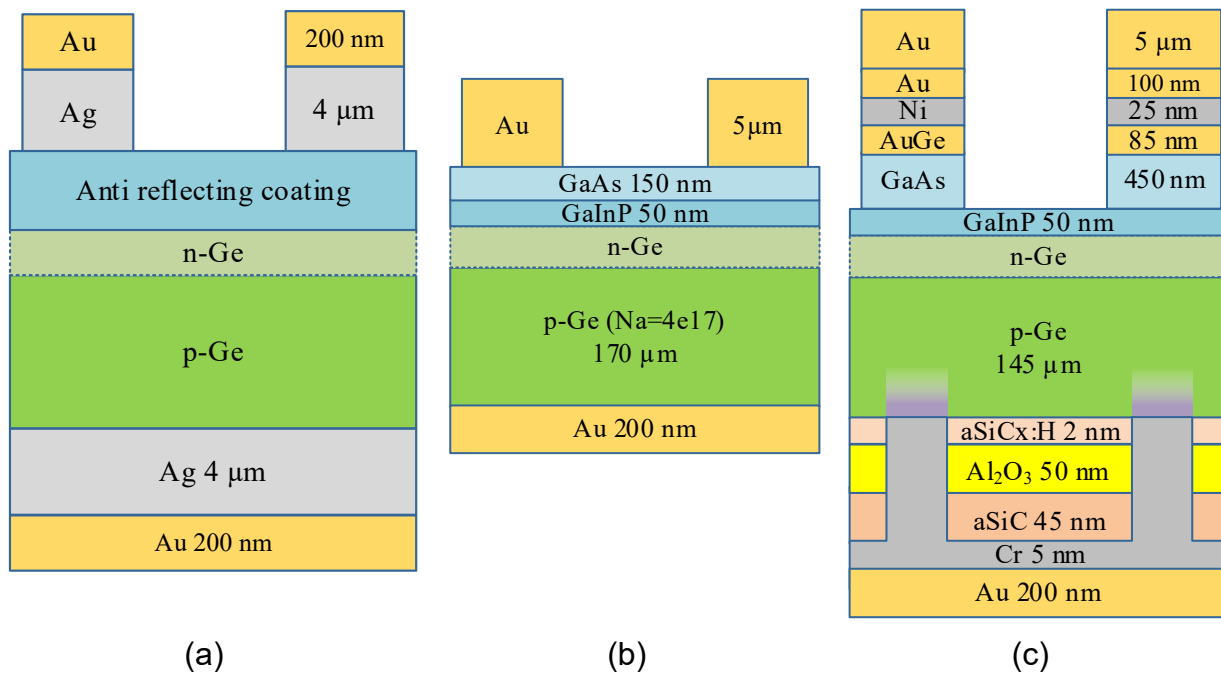


Figure 1. Layer structures of the different Ge TPV cells implemented in the Thermobat Project. (a) Commercial cell, where most fabrication data are unknown. (b) IES-UPM simple cell on highly doped substrate with full rear metallization (denoted as “conventional”). (c) IES-UPM cell fabricated on lowly doped substrate (denoted as “PERC_15”), medium doped substrate (denoted as “PERC_16”), and highly doped substrate (denoted as “PERC_17”), all implemented with laser fired punctual contacts.

As it will be seen later in this report, the commercial cell used in large numbers to implement the latent heat thermal energy storage (LHTES) prototype of this project has lower efficiency and power density than the cells developed at IES-UPM using the laser technique within the framework of this project. Figure 2 shows part of these commercial TPV devices, which were supplied diced, classified, and labeled to ease their identification. The manufacturer provided them with experimental data of the current photogenerated by

each of the 550 samples under the standard extraterrestrial AM0 spectrum (used in the satellite photovoltaic industry).



(a)



(b)

Figure 2. (a) Picture of the commercial 1 cm² Ge TPV cells used in the LHTES prototype. (b) Picture of the front side of the PERC devices fabricated at IES-UPM.

Electrical characterization of I-V curves under dark conditions

The extraction of the I - V curve under dark conditions is a quick and useful characterization technique to perform an initial inspection of the state of the Ge TPV cells either acquired or fabricated. This type of characterization allows a first insight on the potential performance dispersion from a cell population, since it represents the recombination current of the semiconductor device as a function of its bias voltage. This electronic behavior of the p-n junction is fitted using the Shockley equation described by Eq. 1. This expression shows two terms of current, the first one corresponds to the recombination through the p-n junction, where m_1 is called diode's ideality factor (the subindex denotes the possibility of a more complex expression) and I_0 is the reverse saturation current. The second term is determined by the parasitic series and shunt resistances (R_s and R_p). The

rest of the equation parameters: q , k and T are the electron charge, the Boltzmann constant, and the cell temperature, respectively.

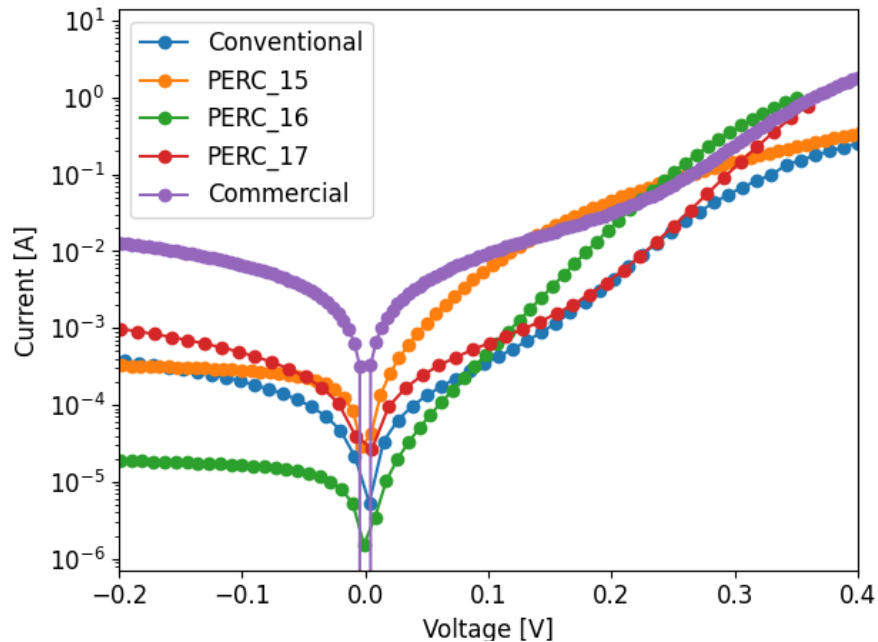
$$I = I_0 \cdot \left(e^{\frac{q(V-R_s I)}{m_1 k T}} - 1 \right) + \frac{V - R_s I}{R_p} \quad \text{Eq. 1}$$

Precise information from each TPV device can be extracted from this dark I - V measurement through the fitting of the Shockley model parameters. Following the superposition principle, which, in first approximation, is commonly applied to photovoltaic devices, most of these same parameters also determine the device performance under illumination when subject to the radiation coming from a high temperature emitter under TPV operation. The quantification of their values will be carried out in the next section, since R_s is dependent on the majority carrier trajectories throughout the device under illumination and therefore, the fitting under such conditions provides more useful information in our case.

Figure 3 shows a set of dark I - V curves that are representative from the three different cell structures (conventional, PERC_15, PERC_16, PERC_17, and commercial), where significant differences among devices can be observed. The result of the dark curve fitting of all these cells can be seen in Table 1, where the parameter values obtained from the fitting to the Shockley equation (Eq. 1) are shown. It is noteworthy that the R_p of the commercial cell is significantly lower than the rest, which can be seen from the slope of the low voltage part of the curve. While this poor R_p is responsible for worse performance of the cell under low irradiance, its deleterious effect can become negligible under high irradiance conditions, as the leakage current through this shunt resistance depends on the cell voltage, and this only increases to a very limited extent, which enables a very small leakage current compared to the photogenerated current (at first approximation, proportional to the irradiance received by the cell). From the rest of the dark I - V curves, it is notable that the R_s of the conventional and the PERC_15 cells is significantly higher than the other cells, which indicates that the processing of both devices suffered from significant problems during their manufacture. This will be easily observable in the reduced fill factor (FF) presented in the corresponding I - V curves under illumination of the next section. It is remarkable that the R_s is relatively low in the PERC_16 and PERC_17 cells, which is a crucial feature for their performance under the very high irradiances typical of high-temperature TPV operation. This will also be verified with the I - V curve characterization under illumination from the next section. Regarding the I_0 parameter, corresponding to device recombination, the PERC_17 and conventional cells present the lower values, being the I_0 of the PERC_16 slightly higher and that of the PERC_15 significantly higher, which can be attributed to the lower doping of the substrate in these two structures. As regards of TPV efficiency, a trade-off exists between the loss in V_{OC} because of the use of a lower doping of the substrate (which implies a reduction of the electrical power output) and the lower transmissivity of the out-of-band radiation produced by the reduced free carrier absorption of this lowly doped substrate (which implies a reduction of the heat dissipated and transmitted by the cell). Further investigation is being carried out to determine the optimum design regarding this trade-off.

Table 1. Parameter values resulting from the fitting of the dark I - V curves.

Device	I_0 [A]	m_1 [ad]	R_p [Ω]	R_s [Ω]
Conventional	$1.680 \cdot 10^6$	1.046	2511	0.386
PERC_15	$2.625 \cdot 10^4$	1.260	> 3000	0.514
PERC_16	$3.123 \cdot 10^5$	1.189	> 8000	0.037
PERC_17	$1.475 \cdot 10^6$	1.048	163.8	0.016
Commercial	$1.639 \cdot 10^5$	1.242	10.2	0.022

Figure 3. Comparison between the dark I - V curves of the commercial cell (purple), the PERC_15 (orange), the PERC_16 (green), the PERC_17 (red), and the conventional cell (blue).

Electrical characterization of I - V curves under high-irradiance flashlight

The measurement of the I - V curve under high irradiance conditions can be useful in anticipating the eventual behavior of the Ge devices before they can be measured in the more time-consuming TPV efficiency characterization system. The experimental setup used to measure these high irradiance I - V curves is shown in Figure 4, where a Xe flash lamp powered by a high-capacity power supply is triggered at the same time as a high sampling rate acquisition system that simultaneously collects the current and voltage signals of the device under test (DUT) and the irradiance data from a calibrated sensor. The DUT is placed on top of a thermally controlled chuck or sample holder, where a vacuum suction line helps improve its thermal contact and eases its electrical contact. The electrical bias of the DUT is made by a voltage source in 4-wire operating mode to prevent spurious voltage drops at the cables, which withstand high currents under this high irradiance operation conditions. The flash lamp, generally made of a Xe arc, reproduces

a spectral content equivalent to the standard AM1.5D solar spectrum, where the irradiance can be selected by either modifying the voltage of the flash power supply or the cell-lamp distance.

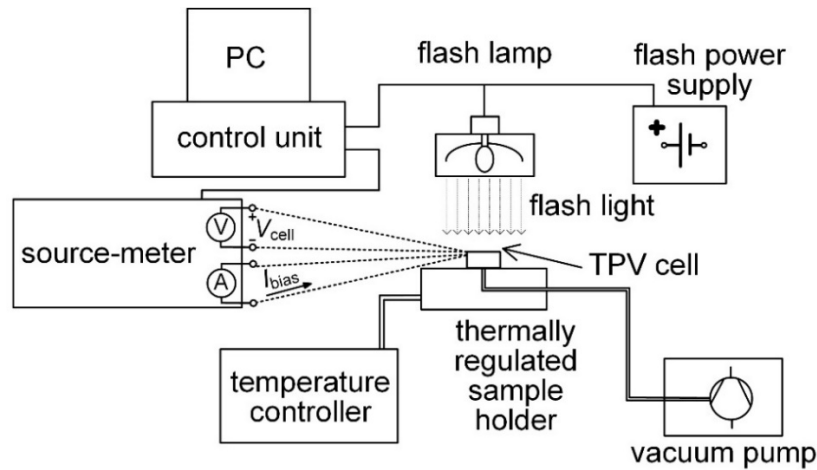


Figure 4. *I-V* curve characterization setup relying on a flash lamp that provides pulsed high-irradiance illumination. The device under test is fixed by vacuum and its temperature is regulated. A 4-quadrant source-meter biases and measures the *I-V* curve at 4-wires.

Figure 5 shows the *I-V* curves of the three samples described above under the action of a concentrated light equivalent to 100 suns. The term “equivalent” refers to the fact that the reference cell is a Ge bottom isotype from a three-junction lattice-matched multijunction cell calibrated for the AM1.5D reference spectrum and therefore, the spectral range absorbed by this sensor is different from the ones in our single-junction cells. However, since this calibrated sensor is always used in all our high-irradiance flashlight experiments, it is useful to provide a reasonable comparison among them.

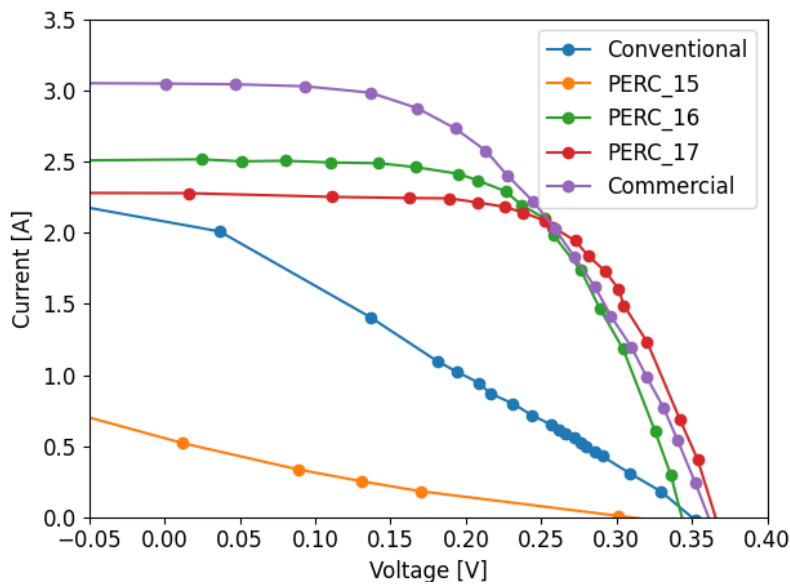


Figure 5. *I-V* curves of the three samples measured at 100 equivalent suns.

As shown in the figure, the FF of the commercial cell is minimally impacted by its poor R_p , as anticipated earlier. This allows us to foresee acceptable operation for this type of device in the LHTES developed in the Thermobat project. It is worth highlighting the high V_{oc} presented by all structures, with the highest value obtained by the PERC_17, closely followed by the commercial cell, and then by the conventional cell, all above 350 mV. The PERC_16 cell has a V_{oc} slightly lower than 350 mV, attributed to the low substrate doping previously discussed. At the same time, it is interesting to note that the series resistance characterizing the PERC_16 cell from IES-UPM, with a value around $13 \text{ m}\Omega\text{cm}^2$ is even better than that of the commercial cell, in the range of $20 \text{ m}\Omega\text{cm}^2$. Consequently, both cells have the same maximum power point, although the V_{oc} of the point contact cell is lower. This is highly relevant for TPV technology operating at very high temperatures, where TPV cells produce large photogenerated currents and a low R_s value can significantly reduce power losses. Additionally, the I - V curve of the conventional and PERC_15 cells exhibit a severely degraded fill factor (FF) caused by a poor R_s of several hundreds of $\text{m}\Omega\text{cm}^2$. Such a large value (one order of magnitude higher than the PERC_16 and PERC_17 cells) is attributed, in the case of the conventional cell, to the degradation of the specific contact resistance of the electroplated gold on its front metal grid, worsened by the inability to perform annealing, due to the thin contact layer of this epitaxial structure. Consequently, poor metal adhesion on both the front and rear cell surfaces, along with a significantly less conductive electroplated gold layer, is likely responsible for the high R_s . This issue was resolved in the PERC_16 and PERC_17 cells by introducing a thicker contact layer in the epitaxial structure, enabling the application of an annealing step after metal deposition. This process improved the specific contact resistance in the PERC batches (except for the PERC_15, which suffered from processing problems which are still being analyzed and in the process of being resolved). Additionally, the improvements applied to PERC_16 and PERC_17, comprised an initial evaporation of a gold layer deposited before electroplating, enhancing adhesion and further reducing R_s . This incremental technological advancement exemplifies the cell fabrication upgrades gradually incorporated through successive design iterations over the past two years to enhance TPV device performance. As a result of these cumulative improvements, both TPV efficiency and power density of our in-house cells have significantly improved, achieving their current high-performance state.

A systematic characterization of flashlight-concentrated illumination was conducted on a large number of commercial cells, enabling the evaluation and classification of their electronic properties. Nearly 100 cells were measured for this purpose, generating experimental data processed using advanced fitting software. Unlike the conventional approach of analyzing a single I - V curve at a specific irradiance, this method considers the fitting of a family of I - V curves across different irradiance levels. This approach allows for a more precise extraction of parameters from the Shockley equation, with a particular focus on R_s , which strongly depends on the photogenerated current. This comprehensive characterization provides an in-depth verification and classification of these commercial TPV cells, a critical step in ensuring the optimal performance of the TPV system. The result is shown in Figure 6, where the values of R_s , R_p , I_0 , and m_1 are represented as a function of the frequency of occurrence for a sample space of about 100 commercial units.

It is noteworthy that the parameter dispersion is relatively small, except for R_p , where some samples have relatively large values, although most of them are concentrated around values below 1,500 Ohms. The central values and dispersions found on I_0 and m_1 are soundly good for the implementation of a performant first prototype of a TPV system showing a large electrical output.

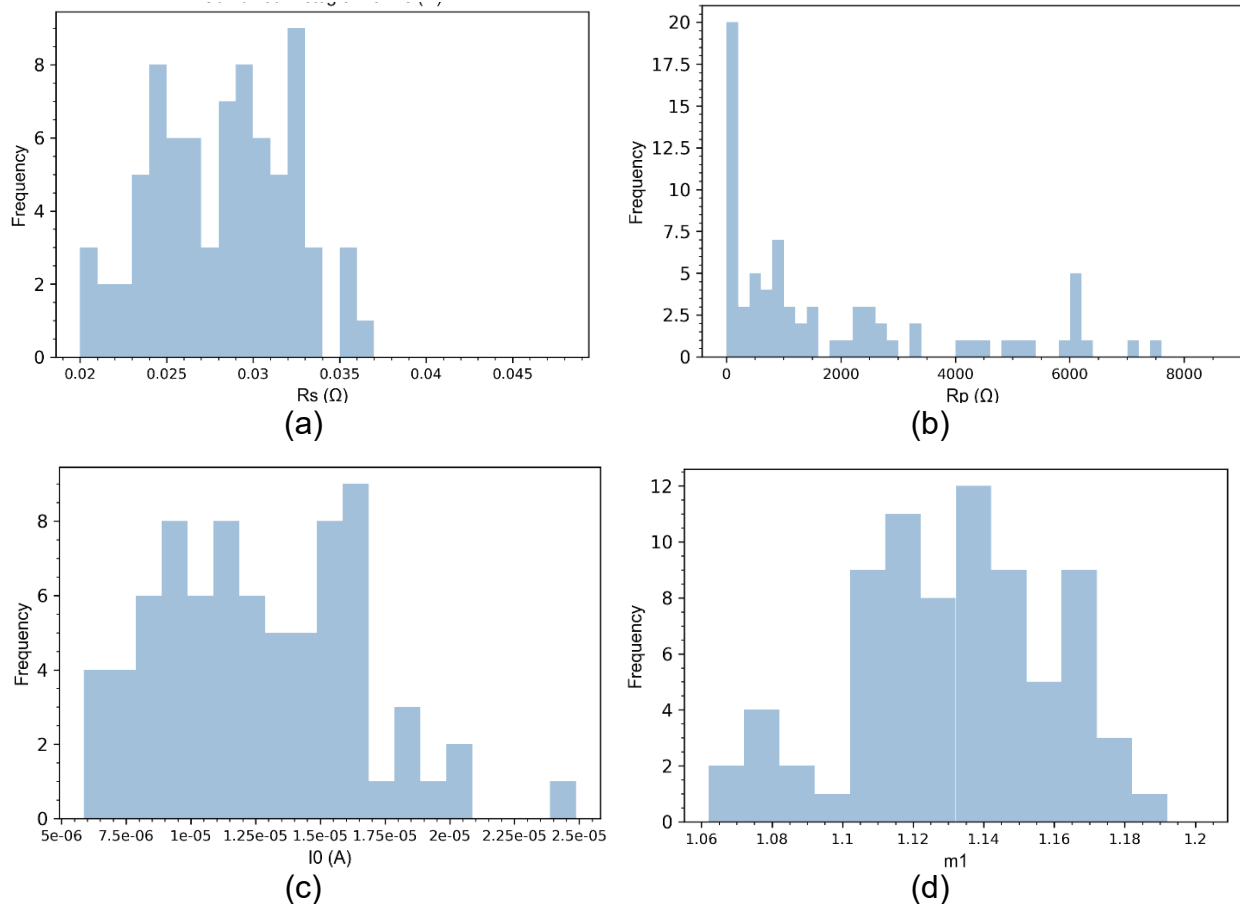


Figure 6. Representation of the frequency of occurrence of the fitting parameter values corresponding to the Shockley equation for a sample space of about 100 commercial devices. (a) R_s . (b) R_p . (c) I_0 . (d) m_1 .

Quantum efficiency characterization

Quantum efficiency (QE) characterization is crucial in photovoltaics as it provides detailed insights into the performance of solar cells. QE indicates the fraction of incident photons converted into charge carriers (electrons or holes) that are extracted through the contacts, contributing to the electrical current. By measuring the QE of a TPV device, the researcher can determine how efficiently it converts the light impinging its surface into electricity throughout the absorption spectrum, identifying losses due to reflection, absorption, or recombination processes. Consequently, QE measurements are essential for optimizing the design and material properties of the TPV cells, leading to the development of more efficient photovoltaic devices.

Figure 7 illustrates a schematic of a synchronous QE characterization system that uses a white light lamp source. A monochromator based on a diffraction grating separates and selects a spectral line, which is then directed to the DUT or a calibrated sensor. To process the signal produced by the monochromatic light, it is modulated by passing it through a chopper. The photogenerated current signals from both the DUT and the calibrated detector are fed into a lock-in amplifier, which selects only the signal at the chopper frequency, thus filtering most of the noise. These data readings are processed and stored by a control unit (a PC in this case), which calculates the numerator of the QE (electrons) from the DUT's electrical response and the denominator (photons) from the current provided by a calibrated detector. This process is repeated for each wavelength (λ) within the TPV cell absorption range.

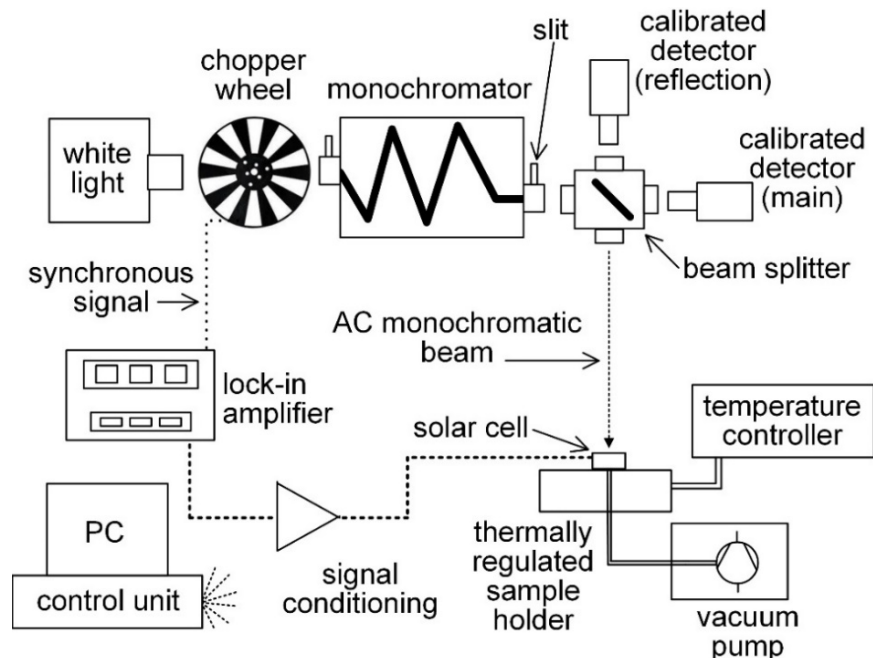


Figure 7. Sketch of the QE setup used to characterize the four types of TPV cells.

The QE signatures of the different Ge TPV cells analyzed in this report have been acquired using a measurement system like the one described in Figure 7. The results of the QE curves obtained are shown in Figure 8. The first thing that stands out is the high QE values of the commercial cell, attributed to the existence of an optimized ARC for this wavelength range. It is also noteworthy that the three cells with laser-fired rear point contacts extend their QE signal several hundred nanometers into the ultraviolet region compared to the other two samples. This is because the GaAs contact layer, which absorbs the most energetic photons (approximately from the 870 nm of its bandgap energy), has been removed during the processing of the PERC structures. Conversely, the conventional and commercial TPV cells have this GaAs contact layer at the top of its structure, producing a sharp drop of their QE signature at short wavelengths. Although, this is expected to have a significant impact on the photogenerated current under AM15D spectrum of the flash characterization system, it will hardly affect the operation under the illumination provided by a high-temperature emitter, as in that case, the spectrum shifts

strongly towards the infrared. Additionally, the QE of the PERC_15 and the PERC_16 sample is also extended in the infrared region, which can be attributed to the better rear surface passivation of this sample, probably related to the reduced doping concentration of the bulk, that is responsible for a higher substrate transparency and makes the effect of the back surface passivation more effective.

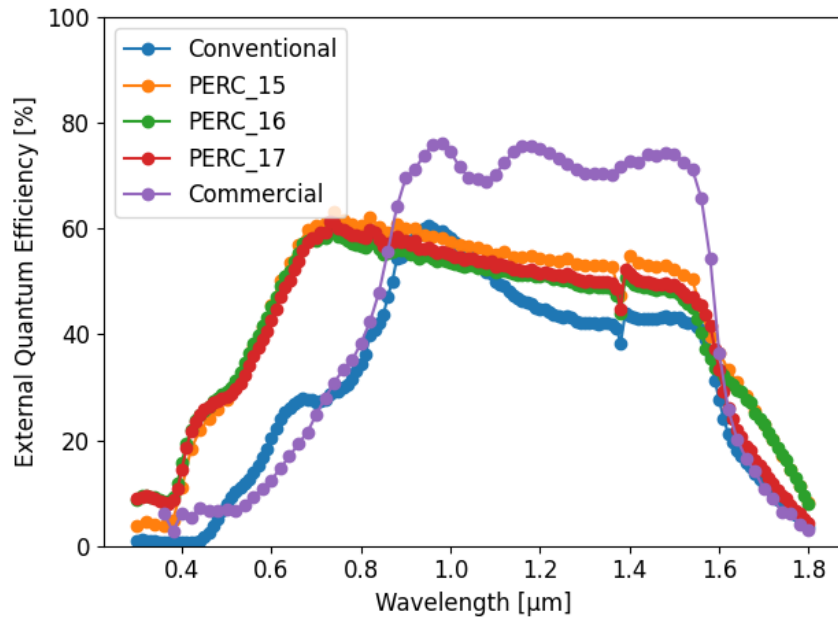


Figure 8. External QE of the five TPV samples measured with the setup shown in Figure 7.

Optical characterization

As explained before in this report, the efficiency of a TPV cell not only depends on the ratio between electrical to illumination power for a given surface, but also on the reflected component of light, which can be sent back to the incandescent TPV emitter. Therefore, the TPV efficiency is highly sensitive to the device's ability to reflect the out-of-band part of the illumination spectrum, which consists of photons with energy lower than the bandgap that cannot be absorbed by the cell. Hence, the optical characterization of the devices is very important, particularly the study of reflectivity in the infrared spectral region on the cell's front surface. This, in turn, will depend on the quality of the rear mirror and its ability to transmit these infrared photons, as they must not be absorbed during their round trip through the substrate.

This type of characterization is carried out using a commercial FTIR spectrometer coupled to an integrating sphere in order to not only analyze the specular component, but every angular component of the reflectivity. This reflectivity is a function of several cell features, such as ARC, portion of the cell covered by metal at the front surface, absorption in the semiconductor or reflection at the rear side mirror. In this case, the reflectivity measurement shown in Figure 9. presents a clearly higher signal for the PERC_16 cell in

the mid infrared range, starting from the Ge bandgap (around 1850 nm). As stated before, this was expected, since the medium doped PERC_16 substrate suffers from a significantly lower free carrier absorption, allowing most out-of-band radiation to be transmitted through the substrate and reflected by the rear mirror. The cells fabricated at IES-UPM include a gold rear mirror, but the mirror of the commercial cell is made of silver. Both PERC cells are expected to exhibit relatively good specularly, aided by the dielectric layers on their rear sides. However, only the PERC_16 cell, with its lower substrate doping and higher transparency, significantly enhances low-energy photon reflectivity. This improvement highlights the substantial efforts invested in successfully optimizing this feature. Completion will include the measurement of the PERC_15, which was excluded due to equipment calibration issues that specifically affected this structure, as it was the last to be manufactured.

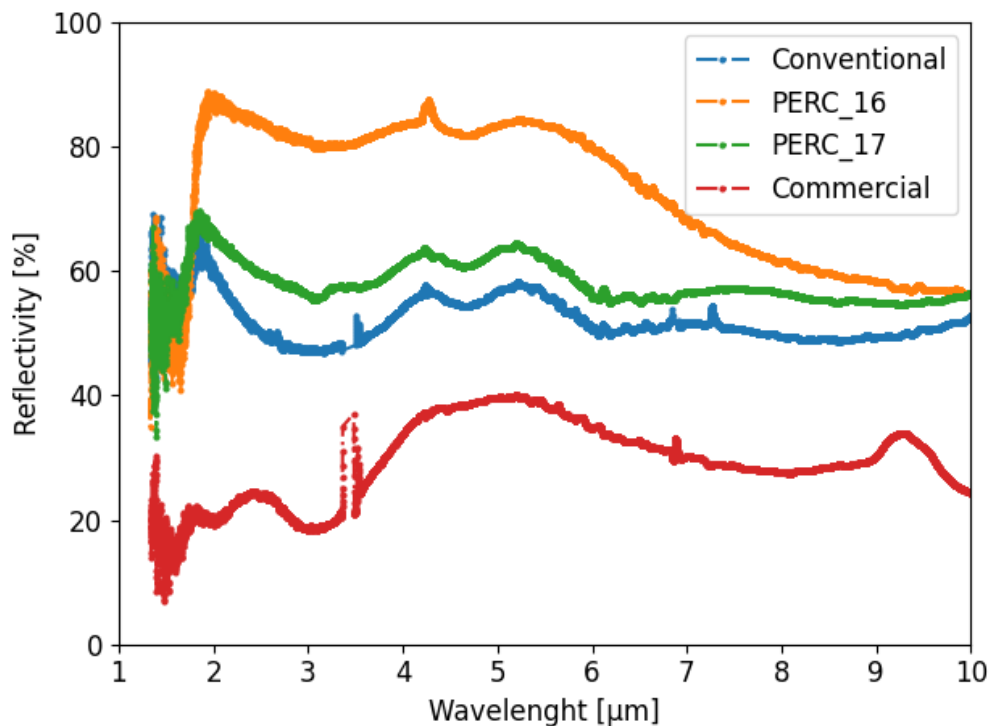


Figure 9. Reflectivity characterization of the four samples obtained by an FTIR setup coupled to an integrated sphere.

Table 2 presents the out-of-band reflectivity values calculated from the reflectivity measurements in Figure 9 for the four devices (conventional, PERC_17, PERC_16, and commercial) normalized to different TPV emitter temperatures: 1000 °C, 1200 °C, and 1500 °C. Overall, PERC_16 confirms the expected improvement, consistently exhibiting the highest reflectivity, with a slight upward trend as the temperature rises. The PERC_17 and conventional devices show more modest reflectivity results, while the commercial cell consistently shows the lowest reflectivity, with a slight decrease as the temperature increases. These trends highlight the enhanced thermal management potential of PERC-based devices with lowly doped substrates.

Table 2. Calculation of the out of band reflectivity normalized to different TPV emitter temperatures.

Device	Conventional	PERC_17	PERC_16	Commercial
Out-of-band reflectivity normalized at 1000 °C	49.6 %	57.0 %	77.9 %	25.6 %
Out-of-band reflectivity normalized at 1200 °C	49.7 %	57.2 %	78.8 %	24.8 %
Out-of-band reflectivity normalized at 1500 °C	49.9 %	57.5 %	79.6 %	24.0%

A quantitative analysis of this optical characterization shows the following trends in the four technologies analyzed here:

- A reflectivity of approximately 50% on average of the conventional cell, a relatively poor value, probably caused by mediocre rear mirror quality added to the effect of a strong infrared photon absorption induced by the highly doped substrate of this reference structure.
- An even poorer reflectivity of approximately 30% of the commercial cell, probably indicating that its substrate is even more doped than the conventional cell or that its rear mirror is not very effective for infrared photons (or a combination of both explanations). However, this result is also affected by the ARC present in this structure. The individual contribution of these elements cannot be determined due to the lack of information on this structure.
- An approximate average value of 60%, representing a modest enhancement of the PERC_17 compared to the conventional cell reflectivity, limited by the large infrared photon absorption caused by the high free carrier absorption in the highly doped substrate, despite the dielectric rear mirror.
- An enhanced reflectivity ranging between 85% and 60% of the PERC_16, obtained thanks to the combination of the dielectric layers constituting a good rear mirror for infrared photons and a lower doping substrate that allows the transmission of the infrared range of the spectrum.

High temperature TPV cell efficiency characterization

The calculation of TPV efficiency (η_{TPV}) differs from that of conventional photovoltaic (PV) devices. In TPV systems, the emitter is positioned very close to the cell, making it necessary to account for radiation reflected by the cell that may be reabsorbed by the incandescent emitter. This reflected radiation is not considered an energy loss in the system. As a result, TPV efficiency is defined as the ratio of the electrical power output (P_{el}) to the total power received from the emitter (P_{in}), minus the power reflected by the cell (P_{out}). Furthermore, the denominator in this efficiency expression, as shown in Eq. 2,

can also be redefined as the sum of P_{el} and the heat lost (or extracted) through the cell (Q_{cell}).

$$\eta_{TPV} = \frac{P_{el}}{P_{in} - P_{out}} = \frac{P_{el}}{P_{el} + Q_{cell}} \quad \text{Eq. 2}$$

Once TPV efficiency is defined, it can be maximized either by extracting more electrical power from the cell or by minimizing heat losses, which are closely tied to the cell's reflectivity. This is especially critical for photons with energies below the cell's bandgap, which pass through the device and are reflected back to the emitter by the rear mirror, a common feature in TPV cell designs. Measuring TPV efficiency is a key figure of merit in the field, as it directly reflects the system's ability to convert thermal radiation into electrical power while redirecting unutilized radiation back to the hot emitter. While the power density a TPV cell can deliver is among its most important characteristics, maximizing TPV efficiency is also crucial for the success of the thermal storage system targeted in this project.

Figure 10 shows a sketch of the TPV characterization setup that has been used in this project [5]. The system uses a laser-heated emitter to irradiate a closely spaced TPV cell that converts part of the radiation received into electricity. The cell is mounted on a copper pedestal with thermocouples measuring the temperature difference between equidistant points along the heat transmission axis. This pedestal acts as a calorimeter to precisely measure the heat flux evacuated out of the cell by conduction, once the convection mechanism has been canceled because the system is under vacuum, and the radiative exchange is negligible because the cell is kept at room temperature through a Peltier cooler that is placed at the bottom part of the calorimeter. The electrical power is extracted from the cell through rear and front contacts and measured at four-wire probes by an external source-meter.

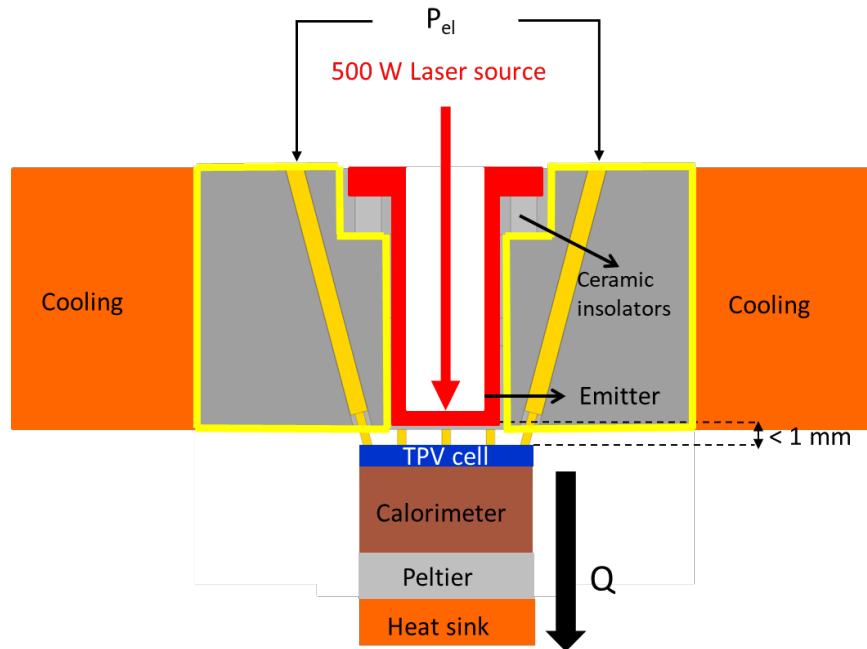
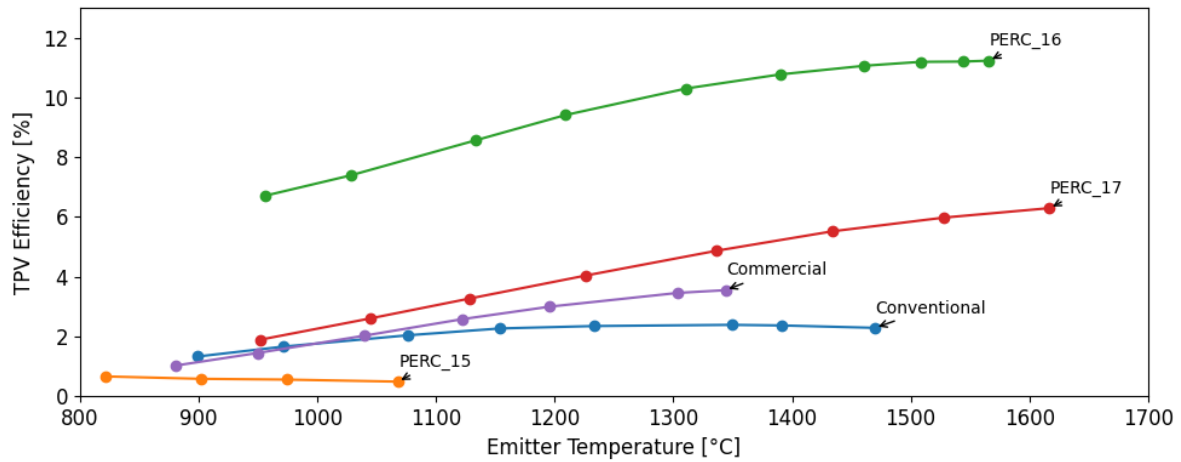


Figure 10. Sketch of the characterization setup used to measure TPV efficiency.

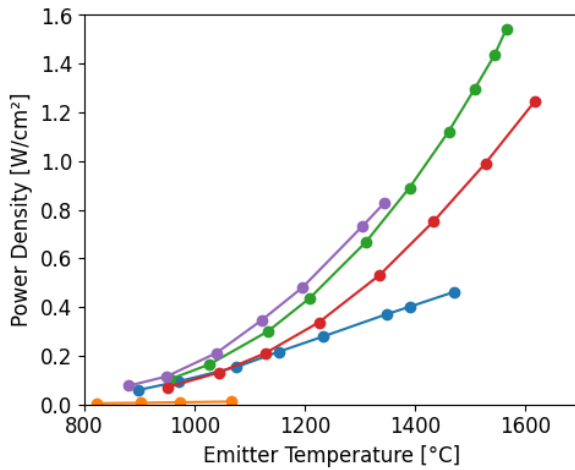
TPV efficiencies have been measured for the commercial TPV cells as well as for those manufactured at IES-UPM. To do this, I - V curves were obtained under different temperature conditions, ranging from 900 °C to over 1,500 °C, as shown in Figure 11. The commercial cell reaches an efficiency lower than 4% at an emitter temperature of 1,350 °C, most probably because it is made with a highly doped substrate and lacks a good back reflector, and therefore, is unable to reflect most of the out-of-band spectrum. Regarding the conventional cell, the efficiency is rather flat throughout the entire emitter temperature range and even lower than the efficiency of the commercial sample, except for the lowest emitter temperature characterized (approximately 900 °C). However, the technological improvements incorporated in the design of the PERC devices, make the high doping substrate sample (PERC_17) significantly improve the TPV efficiency throughout the whole temperature range, reaching a maximum value above 6% at more than 1,600 °C. Moreover, the PERC_16 sample, fabricated with the lowly doped Ge substrate aimed at increasing low energy photon transmission through the substrate and a good quality infrared mirror, demonstrates a notable increase in efficiency throughout the whole emitter temperature range explored. This enhanced performance of the PERC_16 reaches 11,2% TPV efficiency when subject to more than 1,500 °C. As previously mentioned, the poor electrical performance of the PERC_15, attributed to processing issues in this batch, will be excluded from this initial discussion to allow for a separate analysis of the problems affecting this device and to better assess the potential of its proper structure.

To delve deeper into the study of this important characteristic, Figure 11 (b) and (c) also show the power density measured in each of these cells, as well as the heat extracted through the metallic column where the calorimeter is installed and on top of which the cells are contacted and illuminated.

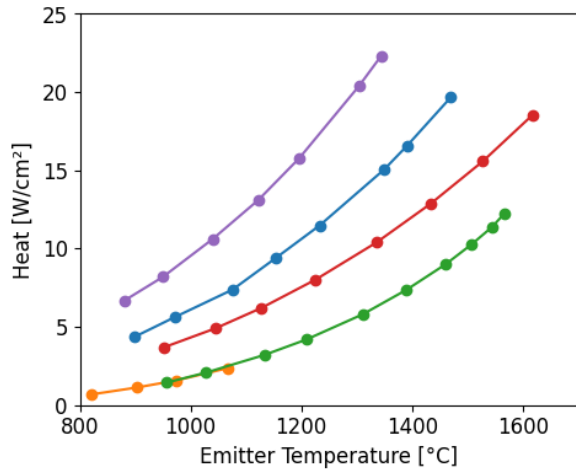
On the other hand, a significant increase in TPV efficiency is observed for



(a)



(b)



(c)

Figure 11. Results from the experimental characterization of (a) the TPV efficiency, together with the data from (b) power density extracted from the cell, and (c) heat generated during the process.

Regarding power density, the commercial cell shows the best performance, probably driven by its greater capacity to absorb the in-band illumination spectrum thanks to the presence of an optimized ARC that produces a significantly larger photogenerated current. In comparison, the devices fabricated at IES-UPM do not incorporate an ARC for the sake of simplicity, obtaining a significantly lower power density.

It is noteworthy that both the commercial and PERC_17 cells present a lower V_{oc} (not shown in the figure) compared to the PERC_16, which can be explained by cell heating during their measurement in the efficiency setup. Consequently, the output power density is slightly reduced in these cells. Regarding the two structures, both show a relatively similar output power as a function of the emitter temperature, except for the lower voltage of the highly doped substrate cell, which is not coherent with the flashlight results (shown Page 23 of 39

in Figure 5). Indeed, the V_{oc} of the PERC_16 is higher than that of the PERC_17, although it typically decreases in cells fabricated with lower substrate doping. Besides variations in cell operation temperature, other fabrication reproducibility issues cannot be discarded. Indeed, the small variability in some cell TPV features, such as in R_s and passivation homogeneity commonly found among devices from the same batch could also help explain these unexpected differences. This can be further analyzed by measuring a larger cell population with the TPV efficiency setup, but it is very time-consuming, and this statistical analysis has not been carried out, since preference has been given to moving forward in the technological improvement of the devices

Regarding the heat dissipated by each of the four structures, excluding the PERC_15, a clear trend is observed in line with the data shown in the reflectivity measurement of Figure 9. In this case, the anticipated effect is verified, whereby the commercial sample drains the largest amount of heat, explained by the fact that it only returns a reduced portion of the photons with energies below the bandgap. The next cell in terms of heat dissipation is the conventional one, followed by the PERC_17, and clearly below all in this measurement provided by the calorimeter, is the PERC_16 cell, which explains an efficiency above 11%. These figures are all in agreement with the optical reflectivity measurements from Figure 9, following the rationale of the improvements achieved in our technology concerning the high-quality rear mirror and the lowly doped substrate.

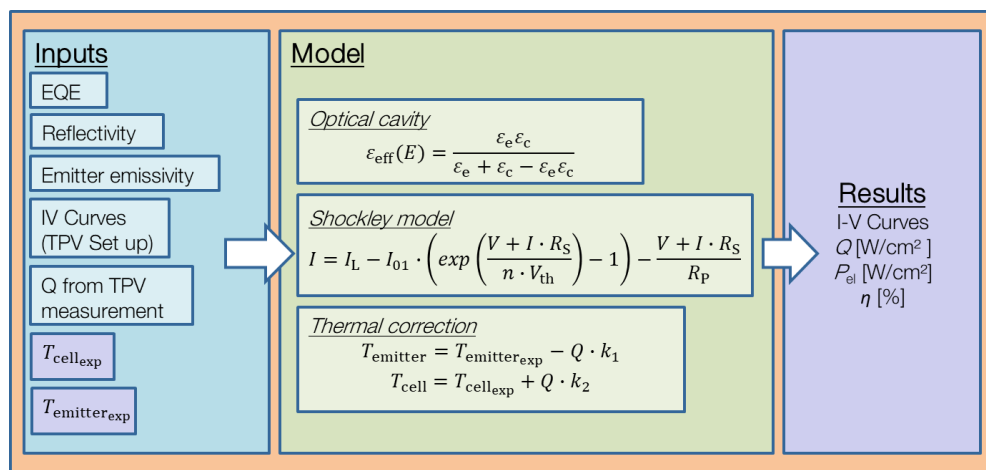
Regarding PERC_15, as previously mentioned, it exhibits poor electrical performance. This structure represents the first fabrication batch, and we anticipate improved electrical performance in subsequent iterations. As shown in Figure 11(c), the heat dissipated in this cell is comparable to that of PERC_16, highlighting good spectral management achieved with the lower doping substrate compared to PERC_16 and PERC_17. However, the heat dissipation was expected to be even lower. Due to the high series resistance of this cell, currently in the range of $700 \text{ m}\Omega\text{cm}^2$, a significant portion of the electrical power output was converted into heat, reducing overall efficiency to the low levels observed.

Simulations and next steps

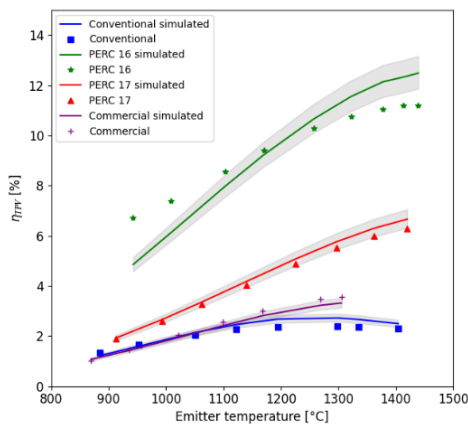
All the design, fabrication, and characterization processes have been supported by the development of a model to fit the experimental data. This analytical model considers experimental inputs for the fitting process such as external QE, reflectivity, I - V curves, heat, emitter, and cell temperatures obtained from the different characterization setups. By integrating the optical cavity effect of two infinite parallel planes, the model recalculates the effective emission across wavelengths for the incandescent source used in the setup in an iterative way. For this, the measured reflectivity of the cell and the emissivity of the emitter are required.

Subsequently, integrating the effective irradiance allows for calculating the effective power absorbed by the cell, considering both in-band and out-of-band radiation. Part of this in-band component is transformed into electrical power and the rest contributes to cell heating. The next step involves using the external QE to calculate to estimate the J_L produced by the cell at a particular emitter temperature. Then, the Shockley equation is

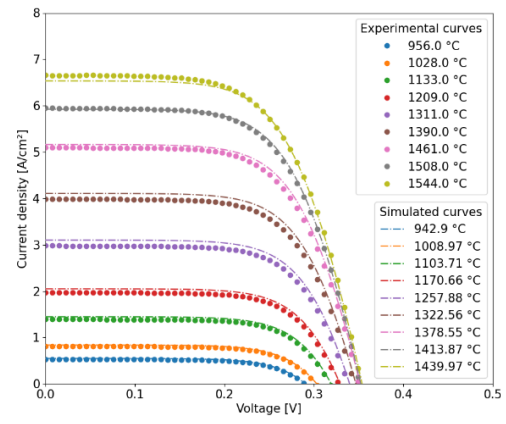
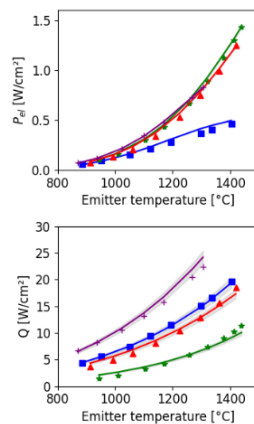
used to calculate the complete I - V curve of the photovoltaic device, which is then compared to the experimental I - V curves, revealing a significant fitting mismatch. To address this, the experimental data of cell heat extraction is used to recalculate the emitter temperature, adjusting it with a fitting parameter (independent of both the cell and the emitter), which finally improves the fitting of the cell I - V curve. A simplified sketch of the model process, including the most relevant inputs, equations, and results is shown in Figure 12(a). It is important to mention that the temperatures actually measured by our thermocouples and pyrometers and the fitting temperatures required by the model to fit the experimental I - V curves data are different. All the experimental temperatures measured at the emitter are overestimated with respect to the emitter temperature values required by the model to obtain proper fittings. Conversely, all cell temperatures required by the model to fit the I - V experimental curves are higher than the temperatures measured experimentally.



(a)



(b)



(c)

Figure 12. (a) Simplified sketch of the fitting model used for our TPV cells operated at high temperature. (b) Results from the fitting of the experimental efficiency, power density, and heat obtained with the model for the TPV samples from conventional, PERC_16, PERC_17, and commercial structures. (c) Experimental I - V curves obtained from the PERC_16 measured with the TPV efficiency setup and fitted with the TPV model at different temperatures.

Figure 12(b) presents the experimental measurements of TPV efficiency, power density, and heat generation for the PERC_16 cell, obtained using the TPV efficiency measurement setup over a wide temperature range. These results are modelled using the previously mentioned TPV system simulation software. The solid lines in the graphs represent the model, which aims to fit the experimental data depicted as small squares. As observed, the model provides an accurate fit for the electrical power generation component, while the fit for heat generation is less precise, likely due to uncertainties in modeling the optical behaviour of the system. Similarly, Figure 12(c) shows the experimental I - V curves measured at different emitter temperatures alongside the corresponding model fits. In this case, the model achieves an excellent fit, accurately reproducing the I - V curves across all temperatures.

Leveraging the models developed within the Thermobat project to guide strategic planning and forecast potential technological advancements, we can adjust input parameters to generate preliminary projections of TPV device efficiencies and power densities as functions of temperature. The proposed next steps center on three critical improvements aimed at enhancing performance:

- Selective emitter integration: replacing the current emitter with a selective emitter optimized to emit high power within the in-band region of the cell's spectrum while minimizing out-of-band emission could substantially enhance efficiency. This modification is projected to increase the efficiency to approximately 15%, aligning with the project's objectives.
- Substrate thinning: reducing the optical path by thinning the substrate to an estimated thickness of 40 μm , without compromising electrical power output, could significantly lower out-of-band absorption. Reflectivity calculations supporting this approach were performed using a custom Transfer Matrix Method (TMM) model. When combined with the selective emitter, this adjustment could potentially raise efficiency to around 18%, as indicated by the model.
- R_s reduction: decreasing R_s aims to improve electrical power output under high irradiance conditions, thereby boosting overall performance. Any enhancement in electrical output would also translate to additional heat extraction from the cell, which could increase the TPV efficiency up to 19%.

By implementing these three improvements, the overall TPV cell efficiency could reach approximately 19% at the maximum operating temperature. It is important to note, however, that these predictions do not account for potential impacts of substrate etching on the external QE. Thus, the projected electrical performance represents a scenario based on current data.

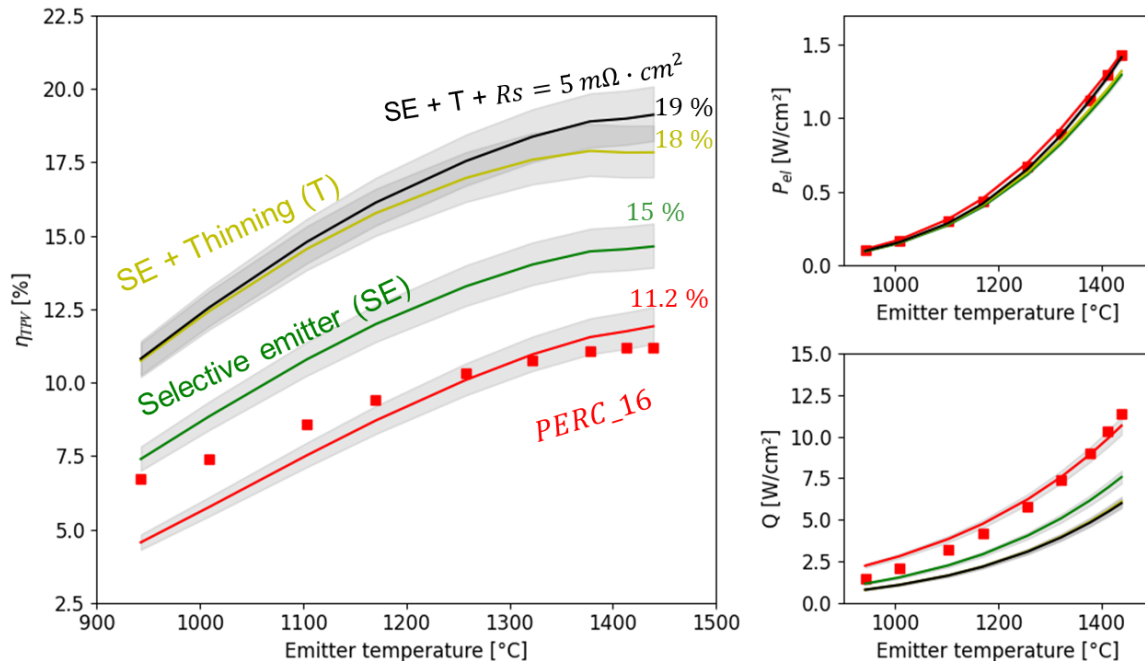


Figure 13. Simulated results of the TPV efficiency, electric power density and dissipated heat obtained with the TPV model considering the current scenario and the potential impact of several TPV cell improvements.

Simulations have been performed for the best of our current cells with the TPV model considering both the current scenario (represented by the red curve, with experimental data points included as a reference) and the potential impact of proposed TPV cell improvements. These improvements, shown in Figure 13, include the use of a selective emitter (represented by the green curve), the combination of a selective emitter with substrate thinning (represented by the yellow curve), and the addition of reduced series resistance (R_s) to the aforementioned enhancements (represented by the black curve). The graph on the left illustrates the TPV efficiency for each of these four scenarios, where the addition of all the improvements projects a TPV efficiency substantially larger than the one targeted in this project. The top-right graph shows the electrical power density, where it is noteworthy that the TPV cell improvements do not enhance the current electrical performance because they are meant to boost TPV efficiency. Finally, the bottom-right graph represents the heat dissipated by the cell under each of the considered configurations. In this case, the projected scenarios reduce significantly the heat flux evacuated by the cell, which in turn leads to the higher efficiencies mentioned before. Together, these simulations provide a comprehensive view of how each improvement could enhance overall system performance under realistic technologically improved scenarios.

Additionally, efforts are being made to complete new fabrication and characterization iterations of PERC_15 and conventional cell with high doping substrate. Unfortunately, due to time constraints and problems related to equipment repair and maintenance in the lab, the batches fabricated so far suffered from processing issues that prevented verifying

the true potential of these cells. Immediate future work is focusing on completing a new iteration of these structures, so that their updated results can be integrated into subsequent deliverables.

Module characterization

The complete TPV module consists of hundreds of interconnected cells, organized into minimodules, which are in turn interconnected, as explained in detail in deliverable D3.2. Each minimodule consists of several cells connected in series and others in parallel, which should produce both a higher minimodule voltage and current. A bypass diode (i.e. a p-n junction device fully metalized in order to prevent photogeneration) contacted in reverse with respect to the cell array interconnected in parallel, is included in each minimodule. This element is intended to prevent a poorly illuminated module from becoming reverse-biased and drain the power generated by other modules. When the photocurrent generated by one of the photovoltaic devices is lower than its series-connected counterparts, its operating point shifts to lower voltages until the current match is produced. However, in the presence of a bypass diode, when the bias voltage of the photovoltaic device reaches the voltage at which the diode starts conducting in forward bias (it must be recalled that the diode's anode is connected to the cell array's cathode and vice versa), most of the current flows through it instead of through the reverse biased photovoltaic device. Thus, when the bypass diode activates, it results in a voltage loss equivalent to the knee voltage of the diode, instead of the potentially high reverse voltage at which the PV device could become biased if no bypass diode were present. However, when the module is properly illuminated and the photogenerated current is sufficiently high for its bias point to be located in the photogeneration quadrant, the bypass diode will be reverse-biased, only producing a leakage current as low as its I_0 , which is typically a negligible fraction of the total current involved.

This deliverable shows the dark and illumination I - V measurements of the bypass diodes, the individual minimodules, and the series association of several minimodules, attempting to reproduce the electrical behaviour that will occur under real TPV conditions in the power generation system corresponding to the LHTES targeted in this project.

Dark I - V characterization

The first measurement corresponds to the bypass diode, which must be able to withstand very high currents in forward bias in case it needs to be activated due to the dysfunctional behavior of the cells to which it is connected. Observing this electrical characteristic up to very high currents, as shown in Figure 14, is a good way to verify the diode's ability to carry a high current without being destroyed or damaged. Such a high current level is equivalent to that produced by the rest of the 5-cell parallel string when operating at a very high temperature. The operation point labeled as (3) shows that a voltage drop of only 0.7 V is obtained when a current as high as 19.87 A flows through the diode, showing an upper limit to the losses that could be incurred in the case this diode is activated to bypass

a poorly illuminated minimodule. This experimental characterization was made possible thanks to the acquisition and commissioning of a new Keithley high-power source-measurement unit in the framework of the Thermobat project resourcing. The dark I - V curve also shows that the forward voltage of the diode is not excessively high, which will limit losses in case it is activated.

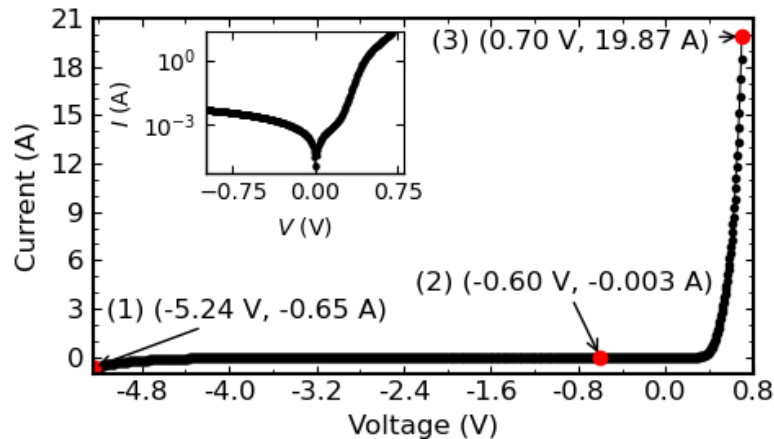


Figure 14. Dark I - V curve of a bypass diode measured up to a very high current by means of a high-power source-meter acquired for this purpose.

After assembling the minimodule and before connecting the bypass diode, its I - V curve was measured in dark conditions, as shown in the green solid line of Figure 15. Then, the bypass diode is connected, and the dark I - V curve of the fully assembled minimodule is plotted with a black solid line. No degradation can be observed together with the expected low voltage breakdown caused by the bypass diode connected in reverse parallel (voltage drop of approximately 0.3 V at low currents), which operates in forward bias in this case. Additionally, the behavior of the Ge TPV is included as a blue solid line for comparison. It is noteworthy that the TPV minimodule presents a significantly higher voltage than that of the individual cell, as expected. Additionally, the reverse voltage breakdown that occurs is very different in the three cases, being higher (in absolute value) in the minimodule without the bypass diode, significantly smaller in the individual Ge TPV cell, and shortest in the minimodule with the bypass diode.

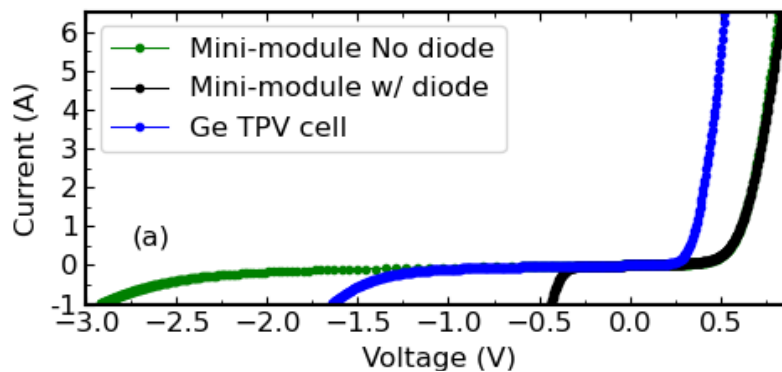


Figure 15. Dark I - V curves of a TPV minimodule comparing the effect of including (or not) a bypass diode and a commercial Ge TPV cell.

Thermal cycling experiments were conducted on the minimodule to evaluate its mechanical and electrical stability under conditions that could potentially lead to degradation from thermal expansion during repeated heating and cooling cycles. The I - V curve was measured both before and after the thermal cycling process, which involved maximum temperatures approaching 100 °C. The results show no detectable differences in the electrical characteristics, demonstrating that the minimodule's assembly is robust and unaffected by the thermal stress induced by this type of cycling. This confirms the reliability of the module design against thermal expansion effects.

Figure 16 shows the different dark I - V curves obtained for a number of complete TPV minimodules, where an apparently high dispersion in the recombination characterization results are observed as a result of the exponential scale of the vertical axis (a linear I - V graph shows almost completely coincident curves). This is probably due to the variability of the R_p previously identified in the characterization of the large population of TPV cells in Figure 6. As mentioned earlier, this low R_p , even when present in the module, does not necessarily pose a problem under TPV operation mode, as the high photocurrents that will be generated will probably mask potential leaks caused by these alternative paths through the junction. Additionally, there is some dispersion in the I_0 parameter of the different minimodules, which will have some impact on the final V_{OC} of these devices. However, this is also unlikely to pose a problem for the overall operation of the TPV system, when these minimodules are interconnected, since the corresponding differences in output voltage of the parallel connected cells are very small, as it will be shown later from high irradiance flashlight characterization. The high current forward region of these I - V curves, dominated by the exponential slope defined by the ideality factor m_1 fitting parameter described in Eq. 1, is impacted by R_s when the product of R_s and I approach the operating minimodule voltage. The dark I - V curves in Figure 16 do not seem to be significantly impacted by R_s , suggesting that the minimodules can be operated at such large current levels with a limited resistive loss (assuming R_s is relatively similar at dark and illumination conditions). Furthermore, the similarity of the high current parts of the I - V curves indicates that there is a relatively low dispersion of R_s and m_1 , as deduced from the statistical results in Figure 6.

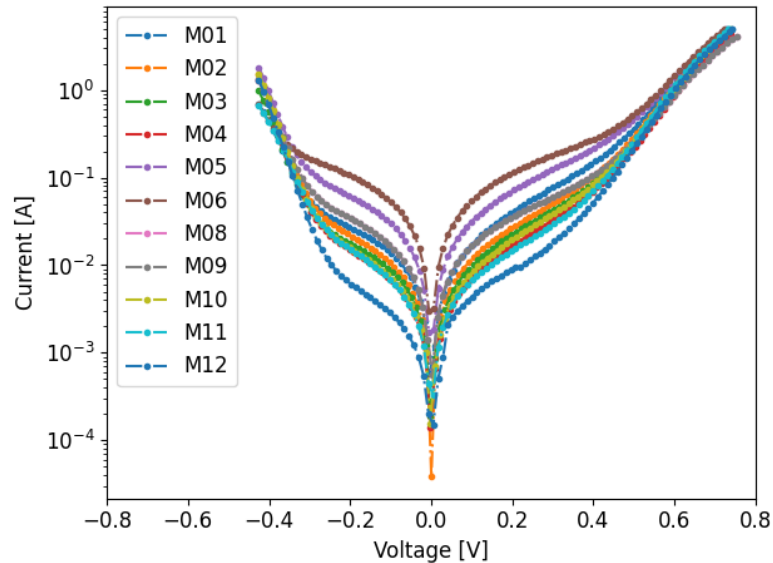


Figure 16. Collection of dark I - V curves of the different minimodules implemented with commercial cells.

High irradiance I - V characterization

The Ge bypass diode was initially characterized under high irradiance conditions using flash equipment, as shown in I - V curve from Figure 17. The results confirm that the photogenerated current density produced by the bypass diode is relatively small at this high irradiance compared to the values generated by the TPV cells, indicating that its contribution to the reduction of the overall minimodule current is negligible. Such photogeneration comes from the fact that these Ge diodes have been processed employing a conservative photolithography process, which leaves some area uncovered by metal at the front surface. This design can be easily improved, leading to a lower J_L and correspondingly lower current losses in the minimodule. Additionally, the forward operating voltage is close to 300 mV, consistent with the dark I - V measurement previously discussed, which is an expected value in Ge devices.

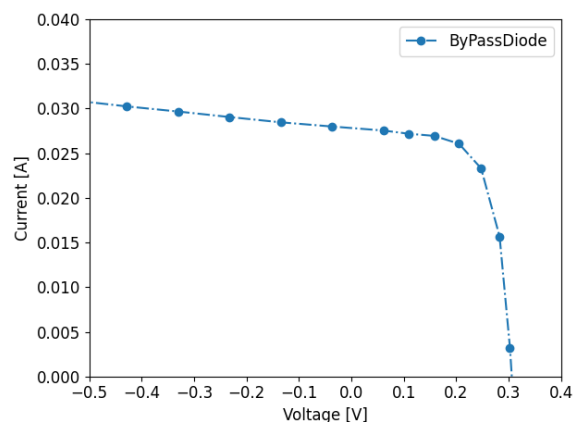


Figure 17. High irradiance I - V curve of the bypass diode.

Once equipped with a bypass diode, the minimodules are expected to demonstrate an electrical response consistent with the cumulative behavior of the individual cells. Specifically, the current scales with the number of cells connected in parallel, while the voltage scales with the number of cells connected in series. This section presents the I - V curves of the minimodule units under concentrated illumination, obtained using the same flash equipment employed for testing the individual cells. As shown in Figure 18(a), the I - V curve of the Ge TPV cell is compared to that of the TPV minimodule, which consists of two series-connected strings, each containing five cells in parallel. Under concentrated illumination equivalent to 100 suns, the results confirm that the voltage of the minimodule is approximately doubled, while the current increases by a factor of about 5. This behavior aligns with the expected series-parallel configuration of the cells within the minimodule.

Furthermore, it is noteworthy that the maximum power measured from the minimodule is nearly 10 times that of the individual cell, with minimal losses. This result is highly encouraging, as it validates the effectiveness of the manufacturing process for the minimodules and highlights their excellent performance under these testing conditions

Figure 18(b) illustrates the electrical behavior of several minimodules characterized under the high-irradiance flash, with I - V curves measured at an illumination level equivalent to 100 suns. The results show remarkable homogeneity across the majority of the minimodules. However, two exceptions are observed: one minimodule exhibits a slight degradation in its FF , while another shows a minor reduction in its V_{OC} . These deviations aside, the overall performance confirms that the fabricated minimodules are well-suited candidates for integration into a TPV system, particularly for applications like the LHTES system currently being developed within the Thermobat framework.

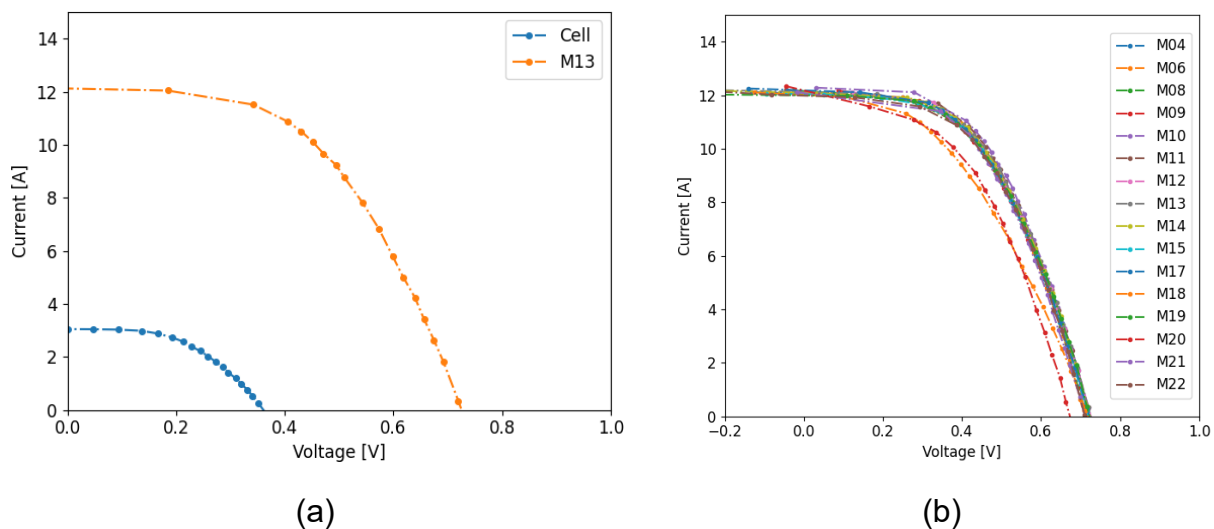


Figure 18. Illumination I - V curves comparing (a) the TPV cell and the TPV minimodule at 100 suns and (b) comparison between the I - V curves of a large number of minimodules at 100 suns.

The systematic measurement of several interconnected minimodules (Figure 19) has also been carried out to evaluate their collective performance when connected in series, as they will be in the final TPV module. The process began with the measurement of a single

minimodule, and additional minimodules were progressively interconnected, one by one, to a total of eighteen. This step-by-step approach allowed for thorough verification of the overall behavior of these interconnected elements, replicating the configuration they will have in practical operation.

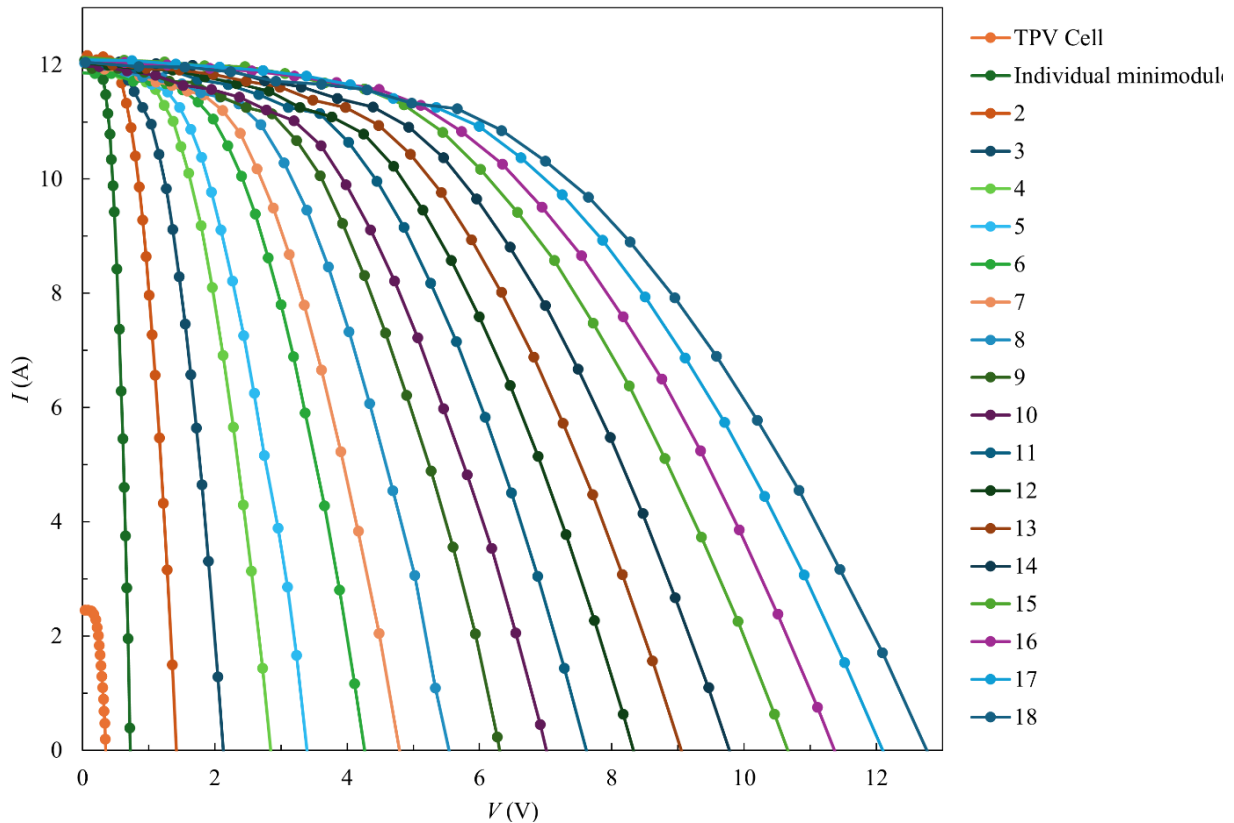


Figure 19. I - V curves under concentrated illumination (100 suns) of the successive series-interconnection of minimodules, from one single element up to eighteen of them.

The results demonstrate that the global maximum power point of the eighteen interconnected minimodules is nearly identical to the sum of the maximum power points of the individual minimodules measured separately, totaling nearly 100 W of output power at approximately 1,400 °C, as it will be shown later in this section.. This outcome is highly encouraging, as it suggests that the TPV system should perform as expected under real operating conditions, with minimal power losses due to interconnection. These findings show the robustness and reliability of the TPV minimodule manufacturing and assembly process for integration into the final TPV system.

Figure 20 presents two key sets of data that provide valuable insights into the behavior of the TPV system. The blue points indicate the emitter temperature (in degrees Celsius) corresponding to the J_{sc} measured for the Ge TPV cell within the TPV efficiency characterization system, reaching currents above 4 A/cm². Meanwhile, the orange points display the relationship between the light concentration (expressed in equivalent suns) applied to the TPV cell and the J_{sc} . This light concentration is determined using a reference cell in the I - V curve measuring system based on flashlight illumination.

This figure establishes a critical link between the photogenerated current and the irradiance (in suns) of the flash lamp system, correlating these measurements with the emitter temperature relevant to the TPV efficiency characterization. The data clearly show that a light concentration of 100 suns corresponds to an emitter temperature of approximately 1,200 °C, while a concentration of 170 suns is associated with a temperature slightly below 1,400 °C. This relationship provides a reliable framework for understanding and relating light concentration and emitter temperature in TPV systems.

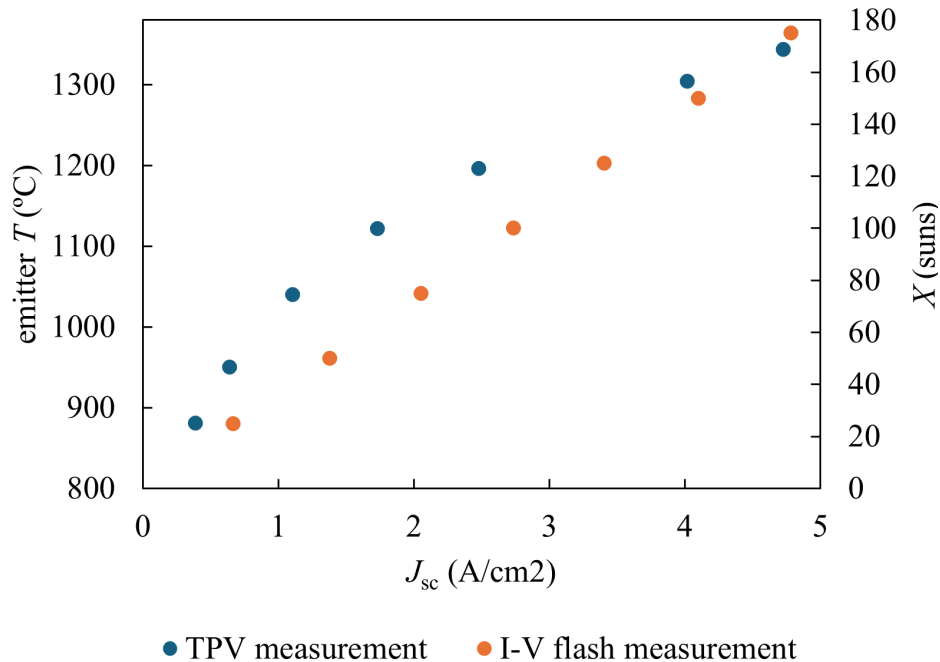


Figure 20. Emitter temperature of the graphite emitter at each J_{sc} (blue dots) and equivalent concentration for the J_{sc} measured in the flash setup (orange dots).

Figure 21 illustrates the total electric power output as a function of the number of TPV cells in operation, measured at various equivalent graphite emitter temperatures. The data provide a clear perspective on how the system's performance scales with the number of cells and the temperature of the emitter. As the emitter temperature increases, the thermal radiation available for energy conversion also rises, leading to a maximum power generated of approximately 100 W for a temperature of 1,400 °C. However, the rate of power increase per TPV cell added to the system vary depending on the specific temperature. This figure is particularly useful for understanding the interplay between emitter conditions and the modularity of the TPV system, highlighting the impact of thermal conditions on scaling strategies.

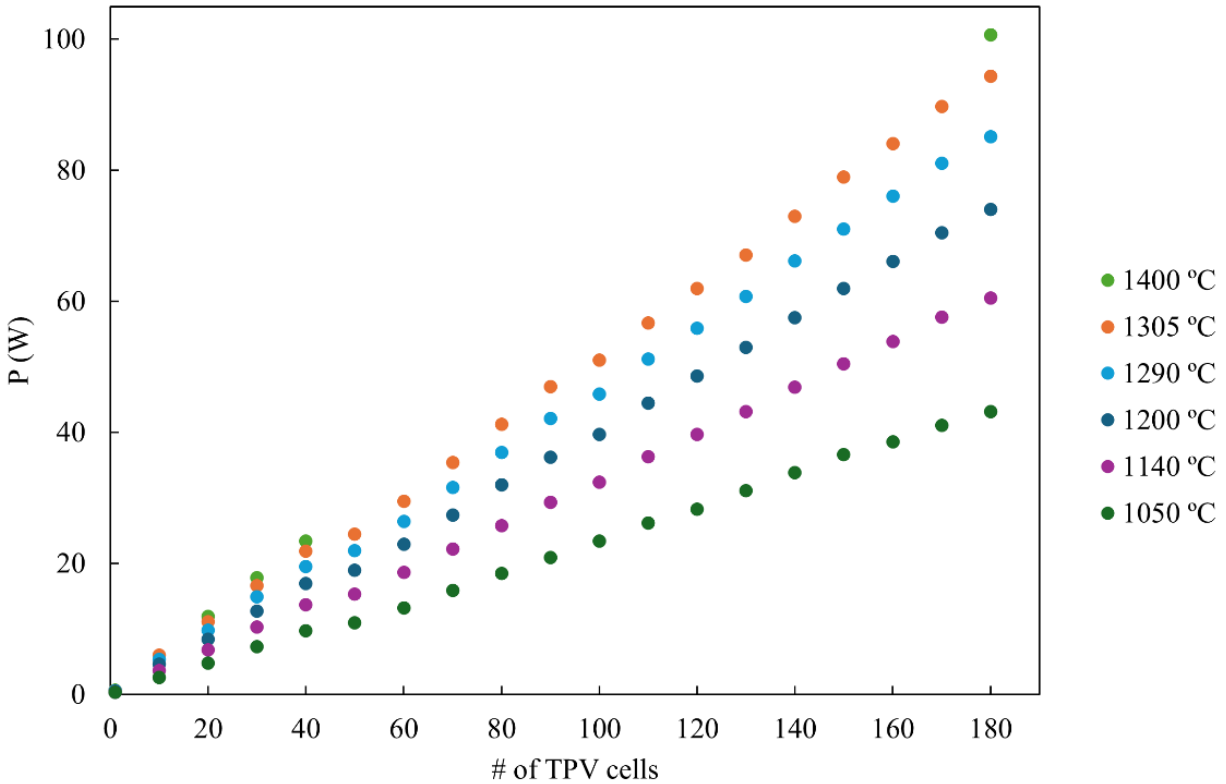


Figure 21. Total electric power as a function of the number of TPV cells measured at different equivalent graphite emitter temperatures.

Thermal characterization

Once the minimodules have been assembled and characterized, a particular experiment is conducted to characterize the temperature effect on the individual Ge TPV cells. For that purpose, a single TPV cell is mounted on a direct bonded copper (DBC) substrate using the same process applied to the minimodule assembly. This new test device is now subject to the high-irradiance effect of the flashlight simulator to obtain the relationship between J_{SC} - V_{OC} at several temperatures. The results are depicted in Figure 22. This measurement is conducted at different plate temperatures to enable the determination of the temperature coefficients alpha and beta (as shown in the datasheet of commercial c-Si PV modules), which describe respectively the variation of I_{SC} and V_{OC} with temperature. These coefficients are crucial for understanding the electrical behavior of the TPV cells under real operating conditions. Specifically, they provide insights into performance at elevated temperatures, which can be expected when the system operates with a very high-temperature emitter or when thermal cooling capacity is somewhat practically limited in actual LHTES systems. This thermal characterization will help refine the analysis of the TPV system's efficiency and reliability under such conditions.

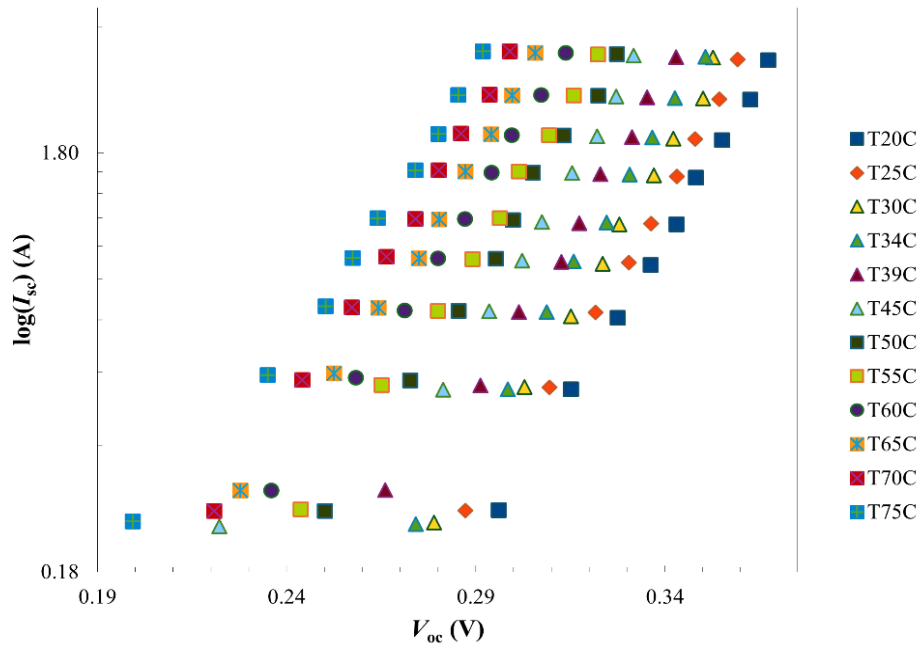


Figure 22. I_{sc} versus V_{oc} at different plate temperatures for a single Ge cell test device.

Finally, to analyse the thermal resistivity of the TPV minimodule stack, the temperature increase as a function of power dissipation through the minimodule was measured, with the results shown in Figure 23. The cell was set at room temperature to ensure that all heat is conducted through the substrate, allowing the electrical power to be approximated as being entirely dissipated as heat within the stack. This thermal behavior was extrapolated from the low-power range, as illustrated in the inset.

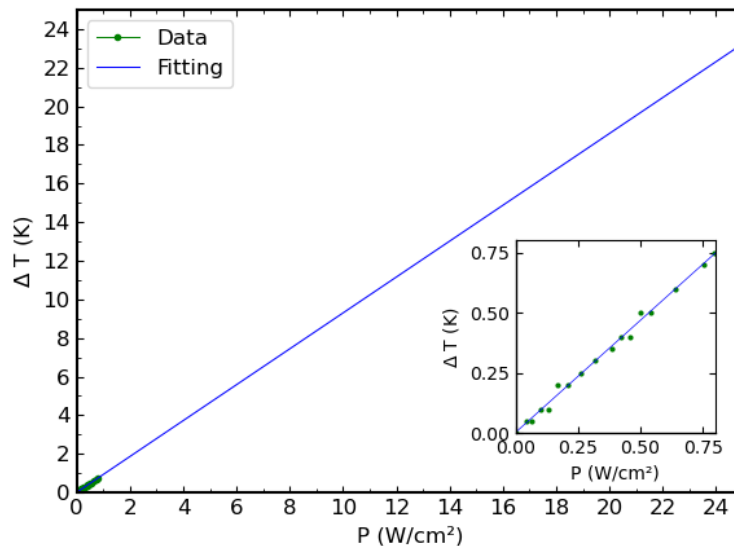


Figure 23. Temperature increment of the DBC stack as function of the power dissipated by the minimodule.

Our commercial Ge cells have relatively low efficiency (slightly above 3%) and must dissipate most of the incoming radiant heat. Considering the relationship between heat flux and TPV emitter temperature, we can estimate the temperature gradient for TPV systems using more efficient cells, such as the optimized PERC₁₆ cell, which achieves a TPV efficiency of 11.2%. As shown in Figure 24, when exposed to an emitter temperature of 1,200 °C, the temperature increase of the PERC cell is only 4 °C, thanks to its ability to convert a larger portion of radiant heat into electricity—significantly outperforming the commercial Ge cell. This improvement is attributed to the PERC cell's advanced features, including an efficient rear mirror and a lowly doped substrate. These characteristics reduce the absorption of infrared photons through free carrier absorption and allow unabsorbed radiant heat to be reflected, thereby minimizing the heat dissipated by the cell.

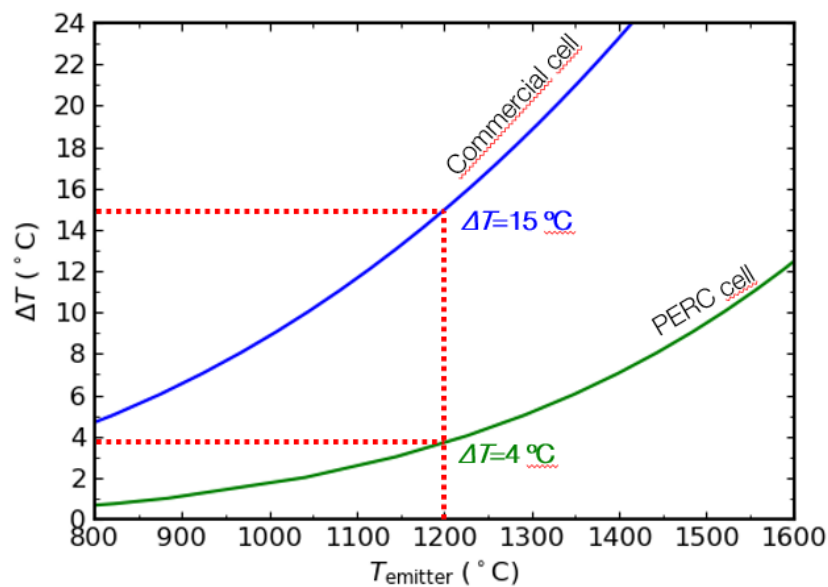


Figure 24. Temperature increment for the commercial germanium cell based minimodule (blue line) and for the PERC cell (green line).

Conclusions

The Thermobat project has made significant strides in advancing TPV technology for high-temperature latent heat storage systems. This report outlines the successful design, iterative development, characterization, and modeling of TPV cells, minimodules, and their integration into a TPV generator. Key findings include:

1. **Enhanced cell performance:** the optimization of rear point-contact Ge-based cells using cost-effective manufacturing processes resulted in a marked improvement in efficiency from 2.3% to 11.2% and an increase in power density from 0.48 W/cm² to 1.43 W/cm² at temperatures above 1,500 °C. The main technological advancements include rear passivating layers, laser-fired contacts, and low-doping substrates.
2. **Electrical and optical characterization:** detailed *I-V* curve measurements, both in dark conditions and under high irradiance, along with QE and reflectivity assessments, have provided crucial insights into the performance and possible degradation of TPV cells and modules. These characterizations are essential for understanding loss mechanisms and guiding future improvements.
3. **Bypass diode integration:** the integration of bypass diodes was shown to be effective in preventing performance degradation of minimodules due to non-uniform illumination, ensuring reliable operation under varying conditions. The same Ge TPV cell epitaxial technology has been used to fabricate the bypass diodes, allowing for a significant reduction of the losses when these elements are activated by inhomogeneous illumination or malfunctioning of some of the series-connected elements.
4. **TPV module performance:** the TPV cells are successfully interconnected, and the quality of the interconnection is validated by the encouraging electrical performance of the TPV minimodules characterized under high irradiance.
5. **Thermal cycling and stability:** the TPV mini-modules were subjected to thermal cycling tests to simulate real operating conditions. The results indicate that the modules maintain their electrical performance despite thermal expansions, confirming their stability and robustness.
6. **Modeling and future progress:** The modeling of the TPV cells, based on experimental results, have allowed forecasting potential improvements in conversion efficiency, which according to our models can approach 20%. At these efficiency levels, techno-economics analysis of the system forecast that LHTPV batteries can be profitable, especially in a combined heat and power (CHP) configuration.

The Thermobat project has demonstrated the feasibility of using Ge-based TPV cells in medium-scale LHTPV battery systems. The advancements in cell efficiency and power density, combined with a thorough understanding of system-level interactions, pave the way for the development of cost-effective and high-performance TPV generators for high-temperature energy storage applications.

References

- [1] A. Datas and R. Vaillon, “Thermophotovoltaic Energy Conversion,” in *Ultra-High Temperature Thermal Energy Storage, Transfer and Conversion - 1st Edition*, Elsevier, 2020.
- [2] T. Burger, C. Sempere, B. Roy-Layinde, and A. Lenert, “Present Efficiencies and Future Opportunities in Thermophotovoltaics,” *Joule*, Jul. 2020, doi: 10.1016/j.joule.2020.06.021.
- [3] A. Datas, A. López-Ceballos, E. López, A. Ramos, and C. del Cañizo, “Latent heat thermophotovoltaic batteries,” *Joule*, vol. 6, no. 2, pp. 418–443, Feb. 2022, doi: 10.1016/j.joule.2022.01.010.
- [4] B. Wernsman *et al.*, “Greater than 20% radiant heat conversion efficiency of a thermophotovoltaic radiator/module system using reflective spectral control,” *IEEE Transactions on Electron Devices*, vol. 51, no. 3, pp. 512–515, Mar. 2004, doi: 10.1109/TED.2003.823247.
- [5] E. López, I. Artacho, and A. Datas, “Thermophotovoltaic conversion efficiency measurement at high view factors,” *Solar Energy Materials and Solar Cells*, vol. 250, p. 112069, Jan. 2023, doi: 10.1016/j.solmat.2022.112069.

Disclaimer

The authors are solely responsible for this information, and it does not represent the opinion of the European Community. The European Community is not responsible for any use that might be made of the data appearing therein.